THESIS FOR THE DEGREE OF DOCTOR OF PHILOSOPHY IN NATURAL SCIENCE, WITH FOCUS ON CHEMISTRY

A Waterborne Colloidal Model System Consisting of Fluorinated Spheres Bearing Grafted PEG: Synthesis, Characterization and Properties

Jeanette Ulama
Institutionen för kemi och molekylärbiologi

Akademisk avhandling för filosofie doktorsexamen i Naturvetenskap, inriktning kemi, som med tillstånd från Naturvetenskapliga fakulteten kommer att offentligt försvaras fredag den 29:e januari 2016 kl. 10:00 i KB, Institutionen för kemi och molekylärbiologi, Kemigården 4, Göteborg

ISBN 978-91-628-9688-1 (print)
ISBN 978-91-628-9689-8 (PDF)
Available online at: http://hdl.handle.net/2077/41127

UNIVERSITY OF GOTHENBURG

Department of Chemistry and Molecular Biology

ISBN 978-91-628-9688-1 (print)
ISBN 978-91-628-9689-8 (PDF)
Available online at: http://hdl.handle.net/2077/41127

Front cover: Cryo-TEM image of PEG-grafted fluorinated spheres suspended in 0.5 M Na_2CO_3.

Printed by Kompendiet
Gothenburg, Sweden 2016

List of Papers

This thesis is based on the following 4 papers and will be referred to in the text by their Roman numerals.

Paper I **Monodisperse PEGylated spheres: An aqueous colloidal model system**
J. Ulama, M. Zackrisson Oskolkova, J. Bergenholtz
J. Phys. Chem. B
118, 2582-2588 (2014)

Paper II **Semi-batch synthesis of colloidal spheres with fluorinated cores and varying PEG grafts**
J. Ulama, K. Jonsson, M. Zackrisson Oskolkova, J. Bergenholtz
Submitted to J. Phys. Chem. B

Paper III **Analysis of small-angle X-ray scattering data in the presence of significant instrumental smearing**
J. Bergenholtz, J. Ulama, M. Zackrisson Oskolkova
http://dx.doi.org/10.1107/S1600576715023444
Accepted for publication in J. Appl. Cryst.

Paper IV **Polymer-graft-mediated interactions between colloidal spheres**
J. Ulama, M. Zackrisson Oskolkova, J. Bergenholtz
Submitted to Langmuir

Publication not included in the thesis

Concentration-dependent effective attractions between PEGylated nanoparticles
M. Zackrisson Oskolkova, A. Stradner, J. Ulama, J. Bergenholtz, *RSC Adv.*, **5**, 25149-25155 (2015)

Contribution report

`Paper I`
The semi-batch method as described was adopted on my initiative. I designed and performed all the synthesis work and all other experimental work (however, with technical help with cryo-TEM and SAXS measurements), and I have contributed to the analysis and interpretation of the results. I wrote the first draft of the paper and contributed to revisions of it.

`Paper II`
I planned and performed the majority of the experimental work. I performed some of the analysis, contributed to interpretation of results, and wrote the first draft of the paper.

`Paper III`
I synthesized the systems used and analyzed some of the scattering data using computer programs from the research group. I participated in discussions of the results and wrote the experimental part of the paper.

`Paper IV`
I planned and performed all the experimental work (however, with technical help with cryo-TEM and SAXS measurements). I performed some of the analysis, contributed to interpretation of results, and contributed to the writing.

CONTENTS

CHAPTER 1

INTRODUCTION

1.1 Colloidal systems

Colloidal particles, here referred to as *colloids*, are in the size range from a few nm to $\sim$1 μm. A colloidal dispersion consists of colloids in a medium where both the colloids and the medium can be in any state, liquid, gaseous or solid. Milk, for instance, is an example when both phases are liquid and is normally referred to as an emulsion. Mist, clouds and smoke are examples of aerosols, where the continuous phase is gaseous and the colloids are either liquid or solid. Colloids are used in everyday life and they are also widely used in industrial processes. In pharmaceutical applications colloids act, e.g., as drug carriers or blood substitutes [1]. In addition, colloids are used in the food industry to give texture and structure to, e.g., milk, butter and jam. In the paper industry, colloids are used as binders and fillers, and in the paint industry they serve as pigments not only for the purpose of adding color, but also to cover the underlying surface [2]. Other examples where colloids play an important role include inks, adhesives and in water clarification [3, 4].

1.2 Model systems

Colloids are not only important in our everyday life and for industrial applications, but colloids have gained interest within the academic community as well. Part of this interest is connected to the fact that the colloidal size range covers many important naturally occurring particles, such as proteins and other biomacromolecules and aggregates of various kinds. Another, very large part of it comes from the industrial importance of colloids, which has motivated the development of the field of *Colloid Science*. A third reason for the academic interest in colloids is that they can be used to mimic the behavior of atoms and molecules to some extent [5]. Since colloids are much larger than actual atoms, with their motion also covering very different time

scales, various experimental techniques can be used to study their behavior such as light scattering and microscopy techniques. To acts as such a model system colloids need to be monodisperse and have well defined size, shape and interaction.

The hard-sphere system is a well studied system both experimentally and theoretically. Here the particles interact via volume exclusion so the interaction is very short-ranged and strongly repulsive. Hence, the colloids should not interact over long distances, but repel each other upon contact [3]. A well studied model system is Polymethylmethacrylate (PMMA) with grafted poly-12-hydroxystearic acid in organic solvent [6]. In a mixture of decalin and carbon disulphide these colloids have been used to study the phase behavior of one-component systems [5] and of colloid mixtures [7]. Another hard-sphere model system is silica particles coated with stearyl alcohol in organic solvent [8]. Electrostatically stabilized polystyrene particles [3] and microgels [9] have also served as colloidal model systems.

Colloidal model systems have been used to study glass transitions [10, 11, 12], phase behavior [5, 13], both short and long-time dynamics which have been studied both theoretically [14, 15, 16] and experimentally [17, 18, 19]. Colloids have also been used to study nucleation and growth of colloidal crystals [20, 21, 22, 23]. Apart from similarities between the colloidal phase diagram and that of atoms, there are also differences stemming from particle polydispersity [24], and the option of controlling size and shape of the both the colloids and their interactions [25]. In other words, colloids are not only useful to mimic atomic behavior, but they display a rich phase diagram of their own including e.g., gels [26, 27, 28, 29, 30] and shear-dependent rheological properties [31, 32].

1.3 Sterically stabilized systems

One common way to synthesize colloids is via emulsion polymerization. The development of emulsion polymerization progressed during World War I and escalated during World War II since synthesizing synthetic rubber was needed due to the shortage of natural rubber [33, 4]. Nowadays colloids of different morphologies such as dumbbells [34, 35], Janus particles [36, 37], and multi-layered spheres [38, 39] can be synthesized. Especially important are polymer-coated spheres due to their robust stability against electrolytes and stability at high particle concentrations. Although colloidal stability is improved, sterically stabilized systems can be destabilized by mechanisms that are not fully understood [40]. Most colloidal model systems are studied in organic solvents, mainly due to the low refractive index of water, so an aqueous colloidal model system would be useful to generalize previous findings.

1.4 Purpose and outline of the thesis

The overall aim of this thesis is to improve our understanding of particle interactions in predominantly aqueous environments and to develop a deeper insight into the relation between particle interactions and collective phenomena. Our goal is to develop and carefully characterize a water-based sterically stabilized colloidal model system. The requirements for an aqueous model system are numerous. Firstly, the particle refractive index needs to be relatively close to that of water. This offers a means to control the van der Waals force and it enables scattering techniques to be used to study high particle concentrations. Secondly, the particles need to be quite monodisperse and spherical to simplify interpretation of scattering data and to enable comparison to simulations and theoretical models. Thirdly, the ability to tune particle interactions in a controlled manner is crucial in order to access various parts of the colloidal phase diagram. Finally, reversible destabilization is sought for to be able to pinpoint the location of phase boundaries. To meet all these requirements, core-shell particles have been synthesized containing a fluorinated core and a polymer-grafted shell. The idea is to use the solubility of the grafted polymer to induce attractions among the grafted spheres and to investigate their collective behavior.

Having introduced the topic and stated the purpose of this thesis we will present the rest of the outline. In Chapter 2, a brief description of emulsion/semi-batch polymerization will be given, followed by a detailed description of the synthesis procedure, including purification of chemicals and post-treatment of the particles. Moreover, we have developed and evaluated a method to transfer the particles from water into simple alcohols. In Chapter 3, we give an overview of the instrumental techniques used throughout this project. We first present a description of the instrumental setup and discuss some key concepts followed by showing some important results. Chapter 4 focuses on colloidal interactions and their link to the phase diagram. In Chapter 5, a brief summary of the four papers included in this thesis will be given. Papers I and II include synthesis and characterization of the colloids with the option of varying the length of the polymer graft. We also synthesized (and characterized) polymer-coated polystyrene spheres. Paper III deals with instrumental smearing in Small Angle X-ray Scattering (SAXS) stemming from the finite size of the beam on the detector. Paper IV focuses on particle interactions and their link to the colloidal phase diagram at low volume fractions. The main conclusions and a few suggestions for further studies are given in Chapter 6.

CHAPTER 2

SYNTHESIS

2.1 Emulsion polymerization

Emulsion polymerization can be either homogeneous or heterogeneous but throughout this thesis we will focus on heterogeneous emulsion polymerization and we also limit ourselves to water as the continuous medium. The key ingredients are a poorly water soluble monomer, a water soluble initiator and a water soluble polymer.

The polymerization process is usually divided into three stages. Particles are formed in stage I. Upon entering stage II, where the number of particles is constant, they increase in size. Finally, in stage III, both the number and size of the particles remain constant. A more detailed description of the three stages is given as follows. The synthesis of latex particles starts with an agitation process to yield monomer droplets and possibly micelles (if surfactant above its critical micelle concentration is present). The initiator, potassium persulfate (KPS), decomposes upon heat to form radicals according to: $S_2O_8^{2-} \longrightarrow 2^{\bullet}SO_4^-$ The sulfate radicals can either terminate or react with monomer (denoted M) in the water phase as described in reaction 1 below. The new radical can either continue to polymerize to form higher oligomers as described in reaction 2 or become terminated as shows in reaction 3. Both the monomer and polymer contain acrylate, so the polymerization occurs via the vinyl group.

1. $^{\bullet}SO_4^- + M \longrightarrow {}^{\bullet}MSO_4^-$
2. $^{\bullet}MSO_4^- + M \longrightarrow {}^{\bullet}M_2SO_4^{2-}$; $^{\bullet}M_2SO_4^- + M \longrightarrow {}^{\bullet}M_3SO_4^-$
3. $^{\bullet}MSO_4^- + {}^{\bullet}M_2SO_4^- \longrightarrow M_3(SO_4^-)_2$

We have synthesized latex with and without a polymeric monomer, referred to as macromonomer, and we have not evaluated the properties of the macromonomer

at 70°C, merely whether it possess surface active properties and has the ability to form micelles. Therefore, we will describe two nucleation mechanisms, one valid with micelles present and the other in the absence of surfactant. The latter is also valid when surfactants are present at concentrations below the critical micelle concentration. The former nucleation mechanism is called SE theory, after Smith and Ewart [41]. The latter was developed by Fitch and Tsai [42] and complemented by the work of Hansen and Ugelstad [43] and is referred to as the HUFT model. A brief overview of these theories will be given and it should be pointed out that the polymerization process is rather complicated.

According to the SE nucleation theory, micelles are only present during the first stage of the polymerization process. Radical oligomers either migrate into pre-existing micelles or form micelles with surfactant molecules. Hence, it is obvious that oligomers themselves can have surface active properties. In the second stage so many particles are present that the probability of new particles being formed is low because all radical oligomers will enter pre-existing particles instead of creating new ones. Hence, particle number is constant during the second stage. As the polymerization occurs within the particles, monomer migrates from the droplets (which act solely as monomer reservoirs) to the particles. This will lead to an increase in the particle size and a decrease in monomer droplet size. The end of stage II is marked by the disappearance of droplets. In the third and final stage, polymerization occurs within the particles and the monomer concentration decreases.

It is obvious that the SE theory fails to describe the nucleation process in the absence of micelles. According to HUFT theory, homogeneous nucleation occurs in the absence of emulsifier. Since no micelles are present, the radical oligomers grow in the aqueous phase until they reach a critical chain length after which they precipitate and become swollen with monomer. Particles grow via coagulation or the entry of other radical oligomers. Since no surfactant is present, particle stability is achieved via residual charges from the initiator. The literature on emulsion polymerization is vast and it remains an active topic of research. For further details on the kinetic and thermodynamic aspects of emulsion polymerization, including a detailed mechanistic approach, we refer to [33].

2.2 Synthesis of core-shell particles

Fluorinated latices have been successfully synthesized in the past using emulsion polymerization [44, 45, 46, 47]. Grafting hydrophilic polymer on latex particles has been done rather routinely, at least for polystyrene and PMMA particles [48, 49, 50, 6], though producing monodisperse polymer-grafted particles is not easily achieved. When it comes to fluorinated particles, however, it has been more difficult to graft these with for instance PEG polymer [51]. Also my own initial attempts, which combined methods to synthesize bare fluorinated particles [46] with

batch co-polymerization of PEG macromonomer used to obtain sterically stabilized polystyrene [50], proved unsuccessful. Only bimodal size distributions were obtained and the polymer grafting density was not satisfactory as judged through stability measurements. We were only able to synthesize monodisperse core-shell particles using a semi-batch polymerization where the initiator was fed slowly into the reaction vessel.

2.3 Semi-batch polymerization

Unlike batch emulsion polymerization where all reactants are added at the beginning of the synthesis, in semi-batch emulsion polymerization only a portion of the reactants are added initially and some reactants are fed separately throughout or partly throughout the polymerization process. The main advantage using a semi-batch approach is the great degree of operational flexibility. Using a semi-batch approach one has the ability not only to control particle concentration and size distribution but also to maintain temperature control. More specifically, particles with core-shell morphology is commonly produced by first synthesizing core particles and adding the second monomer (that would make up the shell) at a later stage [33]. Usually it is the monomer or an emulsion of monomer that is fed continuously, but we have adopted a slow feeding of the initiator to produce monodisperse core-shell particles. Compared to separate addition of monomer, separate addition of initiator has gain little academic interest, but it has been used in emulsion homopolymerization to yield particles with a narrow size distribution [52]. Moreover, the effect of adding the initiator in different ways in the copolymerization of styrene-butylacrylate was used to study the effect on conversion and viscosity [53].

2.3.1 Pretreatment of chemicals

One important factor is to ensure that the purity of the chemicals is sufficient, which we will discuss in detail. The initiator, KPS, is recrystallized in water in the following manner. KPS is placed on a crystallization dish followed by water to create a saturated solution. The crystallization dish is placed in an oven at 40°C until all KPS dissolves. The solution is left to cool slowly at room temperature and further cooling might be required to form crystals (either by placing the solution in a refrigerator or by using an ice bath). The crystals are then suction filtered and washed with ice-cold water. The crystals are left to dry in an oven overnight at 35°C. The dry crystals are transferred to a jar which is sealed and refrigerated for long-time storage.

The monomer, 2,2,3,3,4,4,4-heptafluorobutyl methacrylate (HFBMA), is supplied with an inhibitor (hydroquinone) which needs to be removed prior to starting the synthesis. The inhibitor is removed by passing the monomer through a packed column filled with material for inhibitor removal (CAS 9003-70-7, Sigma-Aldrich). As

a column we use a 2 mL glass Pasteur pipette which we place glass wool at the bottom of and then fill with inhibitor removal resin (∼0.9 g). Glass wool is also placed at the top. If several syntheses are to be made within a couple of weeks it is possible to store purified HFBMA in a refrigerator. The macromonomer, methoxy poly(ethyleneglycol) acrylate (mPEGA480) with an average molecular weight (MW) of 480 g/mol was supplied with both methyl ether hydroquinone (MEHQ) and butylated hydroxytoluene (BHT). The former can be removed using the same column as described above but in order to remove the latter the column was also packed with Al_2O_3. A test was made by purifying the macromonomer with inhibitor removal resin only but this resulted in a bimodal size distribution, so we concluded that the BHT needs to be removed as well. The macromonomer mPEGA2000 with an average molecular weight of 2000 g/mol is a custom synthesis and it was used as received. All other chemicals were also used as received.

2.3.2 Setup

After discussing the treatment of chemicals I now turn to the synthesis procedure. The synthesis setup can be seen in Fig. 2.1. A cold condenser is essential to avoid evaporation of water and monomer so antifreeze is added (giving the condenser its bluish color in Fig. 2.1). The cooling system is typically turned on early in the morning or one day prior to the synthesis. To aid the cooling system further, the level of the final reaction mixture should not exceed the level of the oil bath.

The initiator solution is prepared by dissolving ∼58 mg recrystallized KPS into a 50 mL volumetric flask and filled with Milli-Q water followed by sonication to dissolve KPS and to partly remove oxygen. 10 mL of this solution is later added in a dropwise fashion into the reactor. The macromonomer (if present) is dissolved in Milli-Q water in a 25 mL volumetric flask and also sonicated. Oxygen acts as an inhibitor and therefore the removal of dissolved oxygen is crucial.

In a typical synthesis, 75 mL of water is added to a 250 mL three-necked round-bottom flask which is purged with N_2 for ∼30 minutes at 70°C. The temperature is controlled by having the reactor submerged in an oil bath which is heated on a hot plate. The slow addition of initiator controls the heat release, so temperature control via the oil bath is sufficient. Many objects in a chemical laboratory that are termed "chemically inert" are made of polytetrafluoroethylene (PTFE). However, care should be taken when synthesizing fluorinated latices because polymerization will occur on such surfaces. Therefore, we use a polypropylene stirring blade instead of a PTFE stirrer. Initially we used a stirrer gland but condensation from the reaction mixture mixed with the lubricating oil causing it to seep into the reaction vessel. Therefore, we used a stirrer guide with glass bearings in order to have a leakage-free system.

To maintain an oxygen-free environment, stock grease (with a melting point above

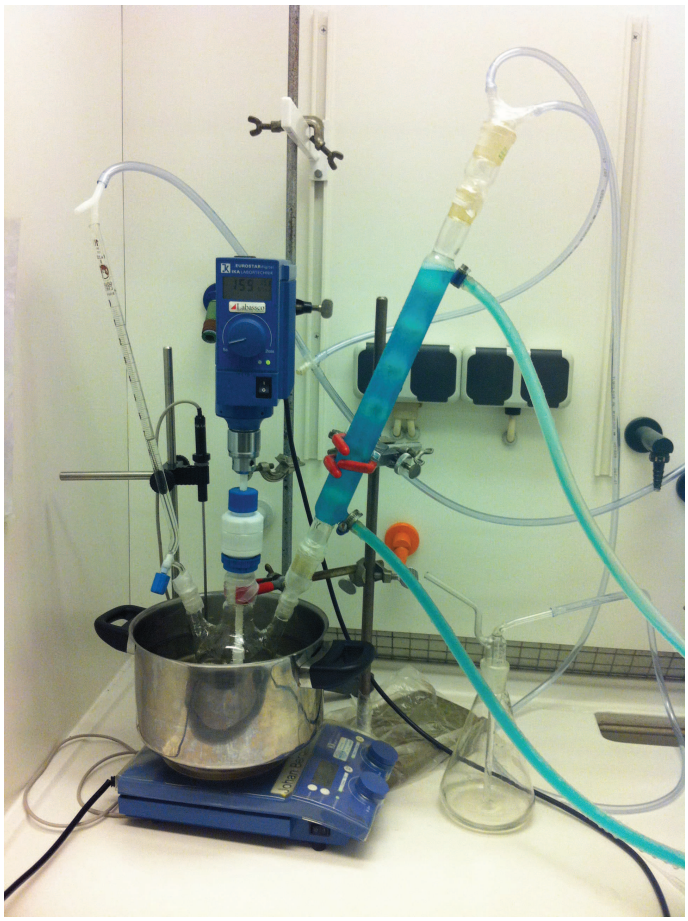

Figure 2.1: Image of the synthesis setup.

the reaction temperature) have been applied to all glass joints. Once the water has been purged thoroughly, the stirring rate is set to 500 rpm and 25 mL of dissolved macromonomer is added followed by 1 mL of purified HFBMA. This vigorous stirring is applied for 1 h followed by a reduction of rotation to 150 rpm and 10 mL of initiator solution is fed dropwise into the reaction mixture. The nitrogen gas outlet passes via a bubble counter in order to avoid any unnecessary stripping of reactants and a nitrogen flow is kept over the initiator to ensure oxygen-free environment (once all the initiator has been added, the nitrogen gas flow can be turned off).

Although it is crucial to feed the initiator slowly into the reaction vessel it is not extremely sensitive towards the speed of the initiator addition. If the initiator is added in a dropwise manner during between 1.5 - 4 h we obtain particles with high grafting density and a narrow size distribution. If the initiator is added too fast a bimodal size distribution is obtained. Adding the initiator too slowly results in a lower yield. The synthesis is turned off after ∼20 h by turning off the heat.

2.3.3 Post-treatment of particles

When the synthesis has cooled down it is filtered twice through a 10 μm filter paper using a B*ü*chner funnel operating under atmospheric pressure. Any unreacted material is removed by dialysis. The cut-off molecular weight of the membranes depends on the molecular weight of the PEGylated macromonomer. For 2000 g/mol or less, it is sufficient to use 12-14 kDa membranes. The dialysis water is replaced daily and progress is monitored by conductivity until the conductivity is similar to that of water. Typically, the first replacements of dialysis water contain much foam which decreases with the number of replacements, signaling removal of unreacted macromonomer. Once dialysis is completed, the batch is filtered through a 0.45 μm nylon syringe filter or 0.45 μm HA membrane filter (Millipore). For long-time storage, sodium azide is added since it is known to prevent bacterial growth [54]. A stock solution of stabilizing media (250 mM) is prepared by dissolving 175 mM NaCl and 75 mM NaN_3 in water and diluted with particle suspensions to yield a solvent with a 1:1 salt concentration of 10 mM in total.

We have used Jumbosep filter devices (Pall Inc., 30 kDa MW cutoff) as a means to make more concentrated particle suspensions and we have ensured particle stability during centrifugation by measuring particle size prior to and after centrifugation using dynamic light scattering. The conductivity of the filtrate did not change during the centrifugation so the ionic strength is not affected. Typically, 50 mL of suspension is centrifuged at 3500 rpm for 2x10 minutes, with refilling of the filter device in between the two runs. The low polydispersity of the particles results in colloidal crystal formation at the bottom of the filter housing. Alternatively, concentrated suspensions can be obtained by bench-top sedimentation. Undisturbed samples form a crystalline sediment within a few weeks.

2.4 Solvent exchange

Advantages using steric stabilized colloids, besides their relative insensitivity against electrolytes [55] and reversible flocculation [56], include their robust stability in both polar and non-polar solvents. This offers the possibility of replacing solvents. I have developed a route for replacing the water with simple alcohols such as methanol, ethanol, 1-propanol and 1-butanol. However, for reasons explained later only methanol and ethanol were successfully replaced. After recognizing that the alcohols have lower densities than water we decided to use centrifugation as a solvent exchange method. As centrifugation tubes we used the Jumposep filter devices (Pall Inc., 30 kDa MW cutoff) to ensure a gentler centrifugation and that the particles remained in the filter housing. We also tested Amicon ultra centrifugal filter units (regenerated cellulose, 100000 NMWL) which worked equally well as a solvent exchange unit. The Amicon ultra units are more advantageous for lower sample volumes but the formation of colloidal crystals in the sample holder makes

it difficult to retrieve the particles, so the Jumposep filter devices are preferred.

Small amounts of water can have a profound effect on PEG dissolved in alcohols [57]. It was therefore crucial to develop a technique to monitor the alcohol content. Our approach was to measure the density of the filtrate and to compare it to a density standard curve of alcohol-water mixtures. The standard density curve was prepared by weighing in specific amounts of water and alcohol which were mixed, taking care to avoid evaporation.

The density was measured at 25°C using a density meter (DMA 5000, Anton Paar). In order to exchange the solvent, a particle suspension was centrifuged at 2000 rpm for 10 minutes and the filtrate was saved. Roughly 15 ml of alcohol was added and then centrifuged again at 2000 rpm for 10 minutes. This step was repeated until the filtrate had roughly the same density as the pure alcohol. The standard curves for methanol/water and ethanol/water mixtures are displayed in Figs. 2.2a and 2.2b, respectively. The red point in each graph correspond to the density of the filtrate and the black lines correspond to linear fits of the respective density standard. According to the standard curves, the alcohol content in the respective filtrate of methanol and ethanol is 99.5%. Since the alcohol content in the filtrate was determined and not the solvent surrounding the particles, we expect the particle solvent to have a minimum alcohol content of 99.5%.

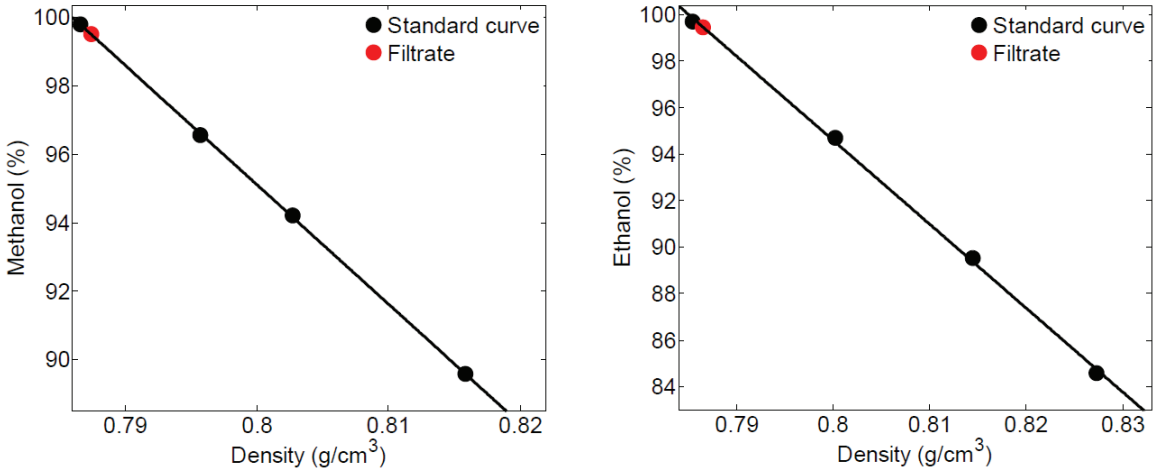

(a) Methanol (b) Ethanol

Figure 2.2: The black data points correspond to the standard curve with linear fits and the red points correspond to the filtrate concentration after 4 centrifugal steps for methanol and 8 centrifugal steps for ethanol.

Corresponding graphs were also made for 1-propanol (data not shown) but long centrifugation times (4x60 min) were needed and invariably particles passed through the filter, signaling filter leakage. Any particles left in the filtrate were filtered off

using a 0.1 μm syringe filter prior to the density measurements. However, not more than 96% propanol was obtained. We were not successful in replacing water with 1-butanol since the filtering devices were not compatible with pure 1-butanol either. Hence the method was only successfully applied when water was replaced by methanol and ethanol.

CHAPTER 3

INSTRUMENTATION

3.1 Ultraviolet-visible spectroscopy (UV-vis)

In UV-vis spectroscopy light of wavelengths ∼200-800 nm is used to illuminate the sample, one wavelength at a time, which excites electrons. Hence, structural information and/or information about electron configurations can be obtained. For our purpose we are only interested in the turbidity so the following description is limited to the transmittance T. When light of wavelength λ with a certain intensity reaches the sample four processes can occur. The beam can be transmitted, i.e. it passes through the sample unaffected. It can also be absorbed, reflected, or scattered, as illustrated in Fig. 3.1.

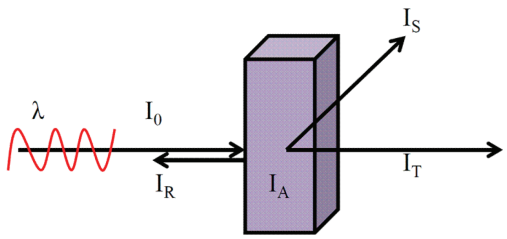

Figure 3.1: Schematic representation over the different processes that can occur when a cuvette is illuminated in a spectrophotometer.

We used spectrometry as a means to determine the refractive index of the dispersed particles. When the volume-averaged refractive index, $\bar{n}_p$, of the particles is equal to that of the solvent, n_f, they become invisible and they lose their scattering ability. This means that the scattered intensity, I_S, approaches a very small value as the match point is approached. For small refractive index differences between the

particles and the solvent, the optical contrast is given by [58]

$$C = 4\left|\frac{\bar{n}_p - n_f}{n_f}\right|^2 \tag{3.1}$$

The so-called transmittance is defined as

$$T = \frac{I_T}{I_0} \tag{3.2}$$

However, we are interested in the point where I_S is minimized. Assuming no absorption or reflection, what is not scattered is transmitted, so the quantity we are interested in is $1 - T$, which is directly related to the turbidity.

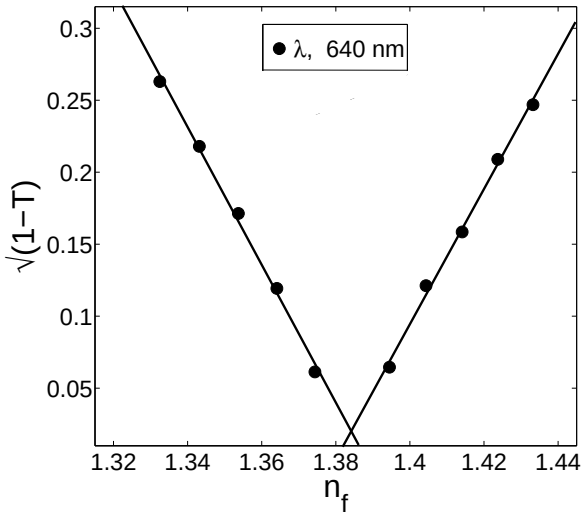

Figure 3.2: Square root of 1 minus the transmittance as a function of refractive indices at a wavelength of 640 nm.

The turbidity is proportional to the optical contrast [58]

$$-T \propto 4\left|\frac{\bar{n}_p}{n_f} - 1\right|^2 \approx 4\left|\frac{\bar{n}_f}{n_p} - 1\right|^2 \tag{3.3}$$

so we expect that $\sqrt{(1-T)}$ should vary linearly with the refractive index of the solvent near the match point. This is verified in Fig. 3.2 where varying amounts of dimethylsulfoxide (DMSO) has been added as a cosolvent to the dispersion with a constant particle concentration to yield different solvent refractive indices. From Eq. 3.3 we know that the refractive index of the particles is given by the minimum in the graph in Fig. 3.2. The solid lines are linear fits to the points below and above the match point. The fitted lines intersect at a refractive index of 1.384. Similar measurements for 2 more wavelengths, 550 and 600 nm, showed that the wavelength dependence of the refractive index of the particles was negligible.

3.2 Dynamic Light Scattering (DLS)

In dynamic light scattering a laser beam is used to probe the particle suspension. In an elastic scattering process, no absorption of light occurs, and the wavelength of the scattered light remains unchanged [58]. Dynamic light scattering is often also referred to as quasi-elastic light scattering, which emphasizes that the shift in wavelength is treated as small [59]. Most materials absorb very weakly for the red wavelengths used in most light scattering applications. As particles move due to Brownian motion, constructive and destructive interference of the scattered light will lead to a speckle pattern in the far field as illustrated schematically in Fig. 3.3. Due to the constant translation of particles, the speckles fluctuate in time. By placing a detector in the far field, the intensity fluctuation as a function of time is recorded. This intensity trace contains both structural and dynamical information. The time dependence of the intensity fluctuation is used to construct an Intensity Auto-Correlation Function (IACF), which in normalized form is defined as

$$g^{(2)}(q,\tau) = \frac{\langle I(q,0)I(q,\tau)\rangle}{\langle I(q\rangle^2} \tag{3.4}$$

When τ, the time separation between recorded intensities, is small, $I(q,\tau)$ will be similar to $I(q,0)$, because particles have not had enough time to move any significant distance. Hence, the intensities are strongly correlated. At long times, $I(q,\tau)$ varies independently of $I(q,0)$, so the intensities are uncorrelated [60].

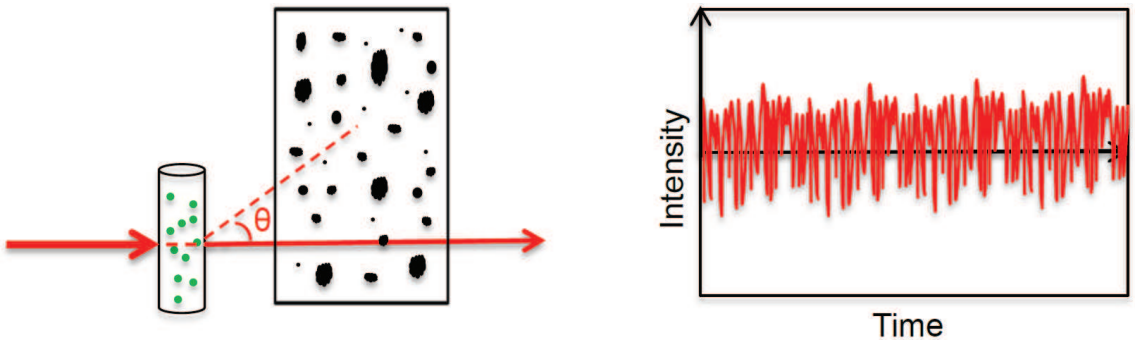

Figure 3.3: On the left: Schematic figure of the scattering, where θ is the scattering angle and the dashed line the scattered light towards the detector. On the right: Schematic figure of the intensity of the scattered light as a function of time.

In Eq. 3.4, q is the scattering vector, defined as

$$q = \frac{4\pi n_f}{\lambda} sin\left(\frac{\theta}{2}\right) \tag{3.5}$$

λ is the wavelength of the light in vacuum and θ is the scattering angle. The IACF is related to an Electric field Auto-Correlation Function (EACF), $g^{(1)}(q,\tau)$, via the so-called Siegert relation

$$g^{(2)}(q,\tau) = 1 + [g^{(1)}(q,\tau)]^2 \tag{3.6}$$

This equation assumes that the detector has an area comparable to that of one speckle. However, only a point detector would have such a property. The finite size of the detector can be accounted for by defining β as an instrument parameter, related to the ratio between the area of the pinhole detector to that of a speckle. If the detector area equals that of a speckle, $\beta \to 1$, and if the detector is so large that several speckles are observed, $\beta \to 0$. In terms of this quantity, Eq. 3.6 now becomes:

$$g^{(2)}(q,\tau) = 1 + \beta[g^{(1)}(q,\tau)]^2 \tag{3.7}$$

This is a very useful relation since it can be used to convert the measured $g^{(2)}(q,\tau)$ into $g^{(1)}(q,\tau)$ which has been analyzed theoretically. The simplest analysis of the EACF shows that it can can be used to obtain information about the dilute-limiting diffusion coefficient, D_0, via

$$g^{(1)}(q,\tau) = e^{-q^2 D_0 \tau} \tag{3.8}$$

The diffusion coefficient can be determined since $g^{(1)}(q,\tau)$ and τ can be obtained from Eqs. 3.7 and 3.8, respectively. Using the Stokes-Einstein relation for spheres

$$D_0 = \frac{k_B T}{6\pi\eta R} \tag{3.9}$$

the hydrodynamic radius R of the particles can be determined. In Eq. 3.9, k_B is Boltzmann's constant, T is the temperature, and η is the solvent viscosity. Equation 3.8 is only valid for truly monodisperse particles since it is fitted to a single exponential. For dilute polydisperse samples $g^{(1)}(q,\tau)$ consists of a sum of exponentials. In 1972 Koppel proposed that the sum of exponentials could be rewritten as a power series expansion, called a cumulant expansion, which is valid if the particle distribution is relatively narrow [61, 62]. It is given by

$$g^{(1)}(q,\tau) = e^{-\Gamma\tau + \frac{\mu_2\tau^2}{2} + \frac{\mu_3\tau^3}{6} + \ldots} \tag{3.10}$$

where Γ is the first cumulant, defined as $q^2 D$, with D the diffusion coefficient, and μ_2, μ_3 are the higher-order cumulants. The second cumulant contains information about the width of the size distribution and the third cumulant controls the skewness (asymmetry) [61].

Dynamic light scattering has been used throughout this thesis in various sub-projects. The main purpose for using DLS has been to extract a hydrodynamic radius but it has also been used to elucidate the scattering behavior of the particles close to the

refractive index match point and to evaluate the stability of dispersions as well as aggregation kinetics.

As an example I include here an examination of how the IACF changes as a function of contrast. The scattering contrast was varied in this case by using ethylene glycol/water mixtures as the solvent. In Fig. 3.4, for the highest concentration of ethylene glycol (91 wt%), which corresponds to a solvent refractive index of ∼1.42, the IAFC mainly displays the usual features of particle translation as expected for dilute dispersions of strongly scattering particles. As the match point of the fluorinated core is approached, a faster relaxation becomes visible. This relaxation is attributed to density fluctuations of the solvent mixture [63, 64]. As seen in Fig. 3.4, almost the entire amplitude of the slower relaxation from particle diffusion is suppressed close to the match point, leaving just the much faster decay from solvent fluctuations. As expected, below the refractive index match point, the particle diffusion process becomes again more dominant as we move away from the match point. Hence, from these measurements the refractive index match point is located between 1.383-1.386, which is in good agreement with 1.384, the result obtained from spectroscopy.

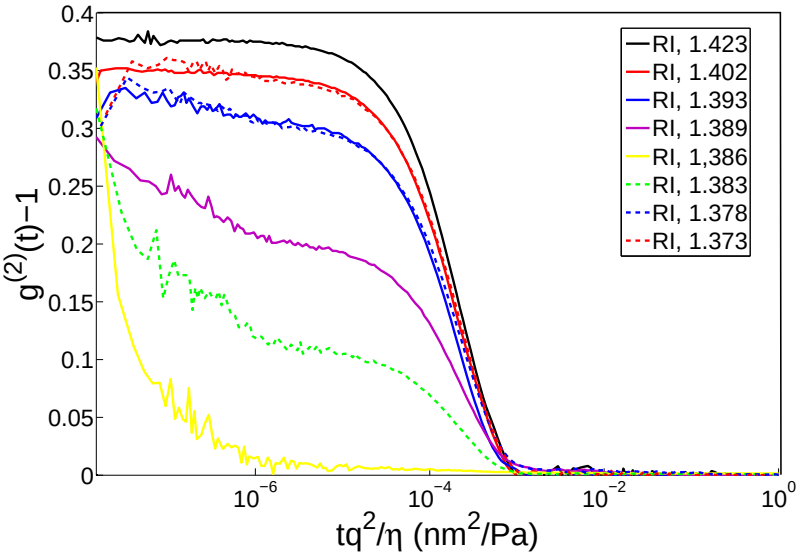

Figure 3.4: Intensity correlation functions in ethylene glycol/water mixtures yielding various refractive indices. The solid and dotted lines are above and below the match point respectively.

3.3 Zeta Potential

A charged particle in a solvent will attract counter ions, which will be situated close to the particle surface. This layer of counter ions is often called the Stern layer and is illustrated as a solid circle in Fig. 3.5 for a negatively charged particle.

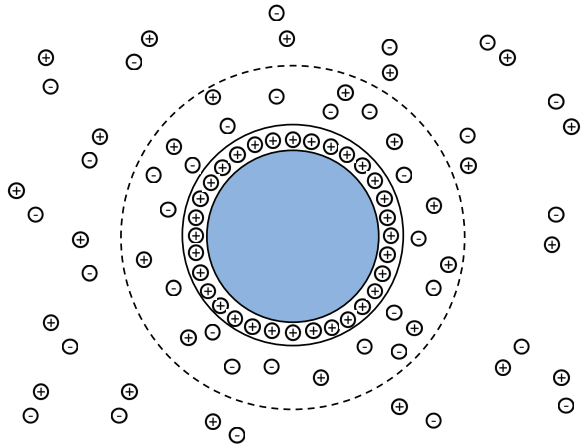

Figure 3.5: Schematic figure of a negatively charged particle in an electrolyte solution.

When placed in an electric field, charged particles will move. The outer layer of ions surrounding the particle, which moves with the same velocity as the particle, constitutes the slipping plane. The slipping plane is visualized as the dotted circle in Fig. 3.5. The zeta potential, ζ, is usually interpreted as the electric potential at the surface of the slipping plane. The zeta potential cannot be measured directly, but it can be calculated through its relation to the electrophoretic mobility, μ. The particle drift velocity, v_d, that results from applications of an electric field is proportional to the electric field strength, E. The electrophoretic mobility is defined as the proportionality constant at low field strengths viz. [65]

$$v_d = E\mu \tag{3.11}$$

The relation between the electrophoretic mobility and the zeta potential, according to Smulochowski [66], is given by

$$\mu = \frac{\epsilon_r \epsilon_0}{\eta}\zeta \tag{3.12}$$

where ϵ_r is the dielectric constant, ϵ_0 is the permittivity of vacuum, and η is the viscosity. This equation is valid if $\kappa R \gg 1$ which corresponds to a relatively large particle at high ionic strength, corresponding to large κ, where κ is the inverse of the Debye length. The Debye length of a 1:1 electrolyte at a concentration of 10

mM is ∼3 nm as obtained through

$$\kappa^{-1} = \left(\frac{\epsilon_r \epsilon_0 k_B T}{e^2 \sum_i n_i z_i^2} \right)^{1/2} \tag{3.13}$$

where e is the elementary charge, n_i is the number density of ions of valence z_i. If the situation is reversed, i.e. for small particles in a medium of low ionic strength, ($\kappa R \ll 1$), H*ü*ckel's equation is valid

$$\mu = \frac{2\epsilon_r \epsilon_0}{3\eta} \zeta \tag{3.14}$$

Since the particles in this work are rather large and suspended in a 10 mM aqueous electrolyte, we use Smulochowski's equation, Eq. 3.12.

Having clarified the relation between the zeta potential and the electrophoretic mobility it remains to mention how a measurement of the electrophoretic mobility can be accomplished. Various types of detection techniques for particle displacements, such as dark field microscopy, electroacoustic techniques, and light scattering, can be used to determine the electrophoretic mobility, but we used detection by light scattering. The same instrument as used for DLS, discussed previously, can be applied using a different measurement cell.

We have used the zeta potential to characterize colloidal surfaces. The initiator, potassium persulfate, leaves negative charges on the particle surface so in the absence of the PEG macromonomer the particle surface will be strongly negatively charged. Polymer-grafted spheres will carry less negative charges due to the presence of PEG and it follows that the zeta potential can to some extent be used to characterize the degree of grafting [50].

3.4 Cryogenic-Transmission Electron Microscopy (cryo-TEM)

Cryo-TEM is a method used to prepare samples which involves vitrification, i.e. transformation into a glass. Vitrification is obtained by cooling a liquid below its freezing point fast enough so that glass formation is favored over crystallization [67].

It should be noted that TEM is an instrument of many components and only an overview of some of them will be give here in a very simplified manner. In TEM, the specimen is bombarded with electrons and the transmitted (or backscattered or secondary) electrons can be detected. In our case we were only interested in transmitted electrons. There are 2 types of electron sources, thermionic (tungsten filaments or LaB_6 crystals) and field emitters (tungsten needles). Thermionic sources, as the name suggests, emit electrons upon heating, whereas field emitters emit electrons

due to high voltage.

After emission, the electron beam passes through a series of condenser lenses, which focus the beam on the specimen and determine the probe size on the specimen. In addition to this, there are lenses that enable the possibility to switch between parallel beams or convergent beams striking the specimen. A parallel beam setup is illustrated in Fig. 3.6.

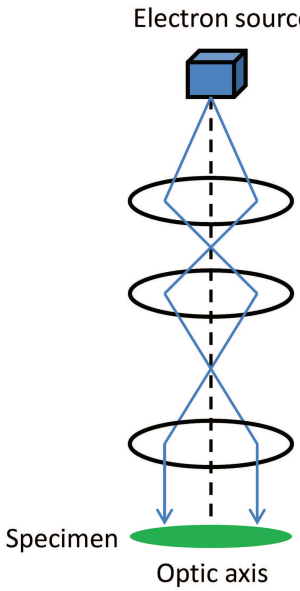

Figure 3.6: Simplified image of the upper part of the TEM setup for a parallel electron beam, where the condenser lenses are displayed as black rings.

Convergent beam setups are used in scanning imaging (STEM), X-ray and electron spectrophotometry analyses and convergent beam electron diffraction. The parallel beam setup is used for TEM imaging and selected-area diffraction. Beneath the specimen is an objective lens which determines resolution and magnifies the image. It is the most important lens of the TEM. The objective lens together with the sample stage is the heart of any TEM instrument. Beneath the objective lens is a series of projector lenses which further magnify the image and can be used to switch between viewing the image or the diffraction pattern. The image is displayed either on a fluorescent screen or on a computer display [68].

We prepared our samples by placing a lacey carbon-coated film on a copper grid support. To avoid evaporation of the sample, the grid is placed in a humid chamber, where the temperature is kept slightly above room temperature. About 5 μL of suspension is placed on the lacey carbon-coated film, and any excess is carefully removed using a filter paper. This procedure fills the holes in the lacey carbon-coated film with suspension. The grid is then quickly plunged into liquid ethane (-180°C)

to vitrify and then transferred to liquid nitrogen (-196°C).

Examples of cryo-TEM images of PEG-grafted pHFBMA particles are shown in Fig. 3.7. The fluorine-containing particle cores are electron rich and appear as quite dark in these images. The PEG layers can be observed in some images, particularly those recorded with higher magnification. Analysis of images such as those in Fig. 3.7 allows for not only determining size distributions, but the thickness of grafted PEG layers can be inferred from nearest neighbor center-to-center separations.

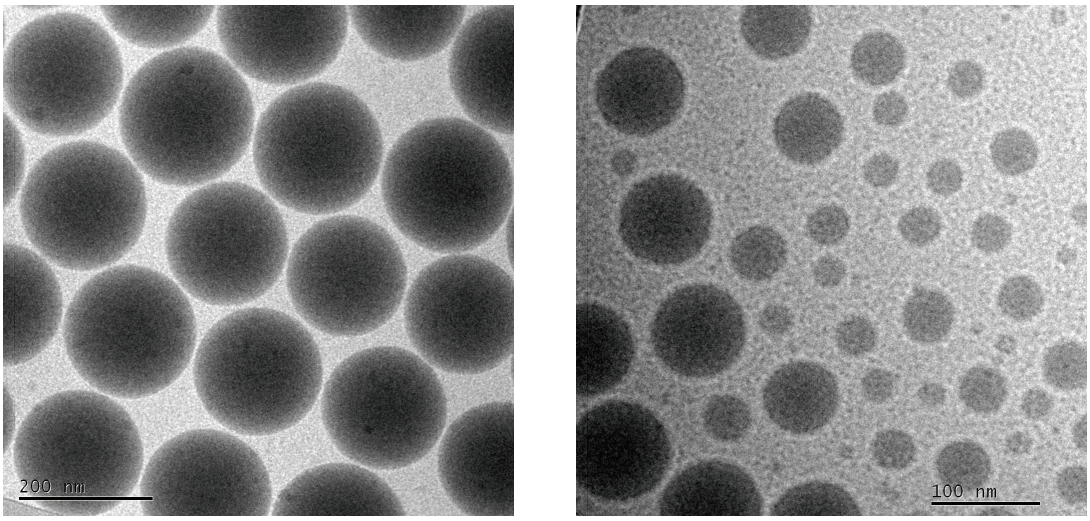

(a) L5 (b) L25

Figure 3.7: Cryo-TEM images of a monodisperse batch (a) and a polydisperse batch (b) of fluorinated latices.

3.5 Differential Centrifugal Photosedimentometer (DCP)

In differential centrifugal photosedimentometry, the time required for particles to travel a certain distance due to sedimentation is used to determine particle sizes and size distributions. A force balance between the drag force, $-6\pi\eta R\frac{dr}{dt}$, and the centrifugal force, $\frac{4\pi}{3}R^3(\rho_p-\rho_f)\omega^2 r$, leads to

$$\frac{\frac{2}{9}R^2(\rho_p-\rho_f)\omega^2 t}{\eta} = ln\frac{r(t)}{r(0)} \tag{3.15}$$

where R is the particle radius, ω is the angular frequency, and t is the time taken to reach $r(t)$, the radial position of the sedimenting particle, which can be written as $R = Kt^{-1/2}$ with

$$K = \left(\frac{9\eta l n \frac{r(t)}{r(0)}}{2(\rho_p - \rho_f)\omega^2} \right)^{1/2} \tag{3.16}$$

In practice, K is determined by using a calibration standard containing particles of known size. The DCP instrument consists of a hollow disc and an absorbance detector at a known distance from its center. The disc is filled with a density gradient (we used sucrose/water mixtures) to avoid bulk settling. The measured absorbance as a function of particle diameter can be converted to a weighted particle distribution by taking the effective light scattering cross section of different particle sizes into account, which is calculated based on Mie theory [69]. The weighted distribution can then be recalculated to yield a number-based distribution. The number-based distributions from DCP were used as a complementary measure of the polydispersity and were also used in optimizing synthesis protocols for obtaining monodisperse particles.

3.6 Small Angle X-ray Scattering (SAXS)

The wavelength of X-rays is between ∼0.1 - 1 nm which means that they can be used as probes on atomic scales.Unlike DLS discussed earlier, conventional SAXS measurements are static experiments so instead of recording the intensity fluctuations as a function of time, the average intensity as a function of scattering vector is measured. The total intensity as a function of q will have a contribution from the so-called form factor $P(q)$, and the structure factor, $S(q)$, as described by

$$I(q) = n_p P(q) S(q) \tag{3.17}$$

where n_p is the number density of particles. Strictly speaking, it is only for systems of monodisperse spheres that the intensity can be divided into form and structure factors, where the former only contains intraparticle correlations and the latter only interparticle correlations.

For a system of monodisperse and homogeneous spheres with radius R and electron density difference $\Delta\rho$, the form and structure factors are given by [70]

$$P(q) = \left[4\pi\Delta\rho \left(\frac{sin(qR) - qRcos(qR)}{q^3} \right) \right]^2 \tag{3.18}$$

$$S(q) = 1 + n_p \int_0^\infty 4\pi r^2 [g(r) - 1] \frac{sin(qr)}{qr} \, \mathrm{d}r \tag{3.19}$$

The form factor depends on the internal structure of the particles, their shape, and size distribution including the size and polydispersity, whereas the structure factor contains information about the positional correlations between particles (and hence particle interactions) through the radial distribution function $g(r)$. $P(q)$ can be

determined under dilute conditions where $S(q) \rightarrow 1$. Knowing $P(q)$, the scattering due to $S(q)$ is given through relation 3.17. To obtain values of size and particle interactions one needs to calculate $P(q)$ and $S(q)$ for a selected model and compare it to the experimental $I(q)$.

In this project we have conducted our SAXS measurements at two facilities, the European Synchrotron Radiation Facility (ESRF) in Grenoble, France and at the Division of Physical Chemistry, Lund University, Sweden. An overview of the ID2 beamline at ESRF is given in Fig. 3.8. The main advantage with the ID2 beamline at ESRF, besides negligible smearing and a far higher radiation flux, is the accessible q-range. At ESRF, the sample-to-detector distance can be varied between ∼1-30 m, while for the laboratory-scale SAXS instrument in Lund the corresponding distance can be varied between ∼0.5-1.5 m.

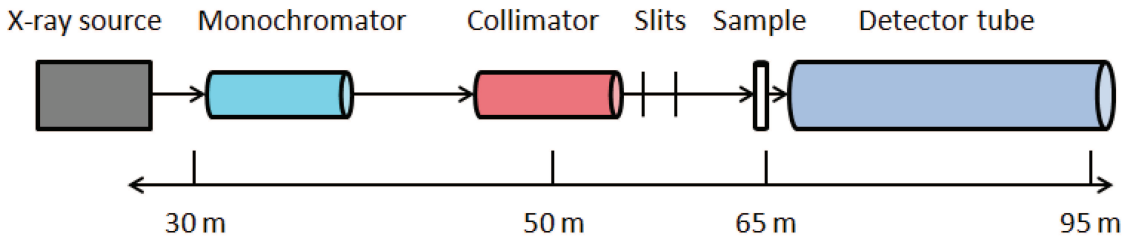

Figure 3.8: A simplified overview over the beamline ID2 at ESRF in Grenoble, France.

CHAPTER 4

INTERACTIONS BETWEEN COLLOIDAL PARTICLES

4.1 Colloids as model systems

There are many types of interaction forces between colloidal particles, but we will focus on the ones relevant to the work in this thesis, hard sphere, van der Waals, electrostatic, and steric interactions. Unlike interactions in molecular systems, colloidal interactions can be tuned. For instance, for the PEGylated particles studied in this work, attractions can be induced upon worsening the solvent quality for the polymer by adding co-solutes such as Na_2CO_3 [71], raising the temperature, [72] or both [73]. The tunability of the interaction enables systematic studies of the link between interactions and macroscopic properties [25].

4.2 Hard sphere

Perhaps the most simple yet for colloids quite realistic interaction is the hard sphere interaction. Here the colloids only interact via volume exclusion, meaning that they occupy space and cannot interpenetrate. For monodisperse particles the interaction is given by

$$V_{HS}(r) = \begin{cases} \infty & r < D \\ 0 & r \geq D \end{cases} \tag{4.1}$$

The hard sphere colloidal phase diagram has been mapped out, yielding fluid and crystalline phases and coexistence between the two [5] as well as a a glassy behavior [12], depending on particle concentration.

4.3 van der Waals

van der Waals forces have different origin namely Keesom, Debye and London interactions, which stem from permanent-permanent, permanent-induced, and induced-induced molecular dipole interactions, respectively. Often, in colloidal systems the London dispersions forces are dominant and one simple way to account for it is to use pair-wise additivity which was adopted by Hamaker [74]. This may be a reasonable approximation for the dispersion interaction, but it is less accurate for polar media which also require consideration of Keesom and Debye interactions. As an alternative, Lifshitz and co-workers [75, 76] described the solvent and particles based on their macroscopic properties such as refractive indices and dielectric properties. In a simplified form, the Lifshitz-Hamaker constant can be expressed as [77]

$$A_{131} = \frac{3}{4} k_B T \left(\frac{\epsilon_1 - \epsilon_3}{\epsilon_1 + \epsilon_3} \right)^2 + \frac{3 h v_e}{16\sqrt{2}} \frac{(n_1^2 - n_3^2)^2}{(n_1^2 + n_3^2)^{3/2}} \tag{4.2}$$

where indices 1 and 3 correspond to particles and solvent, respectively. v_e is the main absorption frequency in the UV region, which is on the order of $3x10^{15}$ s^{-1}, and h is Planck's constant. As a further approximation, the Hamaker constant in Eq. 4.2 can be used in the Hamaker-summed expressions for the interactions between particles of various shapes [77].

The usual interpretation of Eq. 4.2 is that the first term mainly stems from the classical contribution (Keesom and Debye interactions), whereas the latter derives from London dispersion forces. Due to the electrostatic origin of the first term, this can be minimized by the addition of electrolytes due to screening [78], and the latter term is seen to be minimized under refractive index matched conditions. Colloidal van der Waals forces are almost always present in suspensions, but with a suitably chosen system there are ways to control them. This can aid the understanding of the contribution of van der Waals forces to the total interaction.

In a suspension, colloids are constantly bombarded with solvent molecules which push the colloids around in the solvent, which is referred to as Brownian motion. This thermal motion is typically not sufficient to keep particles from aggregating under the influence of van der Waals forces. If colloidal stability is to be obtained, a repulsive force needs to be present to counteract them. We will discuss two such stabilizing mechanisms, electrostatic and steric stabilization.

4.4 Electrostatic interactions

Electrostatic interactions between like-charged particles are generally repulsive and can be of long range. The range of the interaction can be tuned by the addition of electrolyte. This screening behavior is captured by the screened Coulomb interaction that has the form of a Yukawa pair potential [25]

$$V(r) \approx \lambda_D \frac{e^{(-\kappa r)}}{r} \tag{4.3}$$

where λ_D is a coupling parameter that depends on the charge or surface potential of the particles and r is the distance between the particle centers. Recalling Eq. 3.13, the inverse Debye length, κ, depends on the salt concentration and serves to screen the electrostatic interaction.

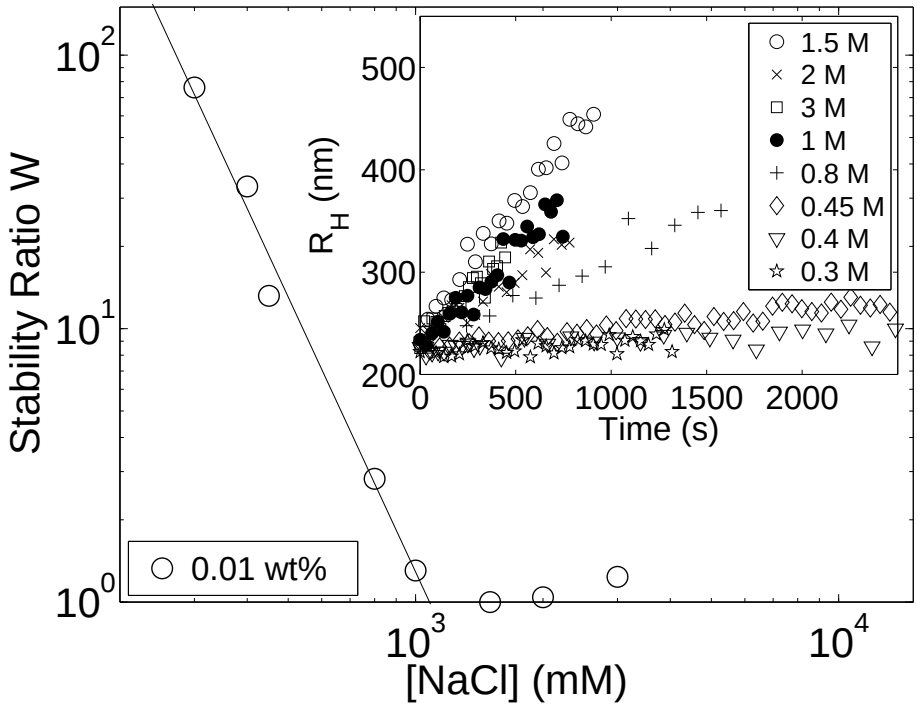

Figure 4.1: Stability Ratio as a function of [NaCl] for charge-stabilized particles without PEG. The inset shows the initial aggregation rate, that is, particle diameter as a function of time for various [NaCl].

At low electrolyte concentrations the interaction is long-ranged, which can even cause particles to crystallize at volume fractions as low as 0.002 [79]. On the contrary, the screening by electrolyte compromises particle stability. This effect is shown in Fig. 4.1 for non-grafted pHFBMA particles with a radius of 227 nm. They carry negatively charged surfaces due to residuals from the initiator. The inset in Fig. 4.1 shows the apparent particle diameter as a function of aggregation time for various NaCl concentrations as determined by DLS. The ratio between the fast aggregation at high salt concentrations versus slow aggregation rate at lower salt concentrations is used to construct a stability ratio, which is shown in Fig. 4.1 as a function of

NaCl concentration. A critical coagulation concentration can be extracted from Fig. 4.1 as about 1 M NaCl. The critical coagulation concentration has also been studied at two lower particle concentrations (data not shown), and it was found to be independent of particle concentration, which is the expected behavior [80].

It is quite remarkable that these charged particles can withstand such high salt concentrations without entering a fast aggregation regime. For similar fluorinated charged spheres, Koenderink et al. [46] saw no aggregation until more than 400 mM NaCl was added, which is in good agreement with the results shown here. One explanation is the low refractive index difference between the particles and the solvent which lowers the van der Waals force [46]. The refractive index of the fluorinated latices is 1.386 [45], and the refractive index of 0 - 3 M NaCl solutions varies between ∼1.33 - 1.36. In other words, the particles are not totally refractive index matched with the solvent and this results in a small but finite Hamaker constant. What remains to be explained is the broad region of slow aggregation, which cannot be done using DLVO theory alone.

4.5 Steric interactions

Interactions between particles with grafted or adsorbed polymer are controlled by the solvent quality for the polymer. Good solvent conditions, which cause polymers to become highly solvated, result in repulsive interactions between particles. This effect is well understood [81, 82]. Interpenetration of layers reduces the volume available to polymers and limits the number of configurations, which results in a repulsive interaction. For poor solvent conditions the situation is considerably less well understood. It is well known that particles aggregate under such conditions, which is a process often referred to as flocculation. The mechanism behind the attraction that must be present has not yet been clarified. There are a number of different proposals. One possibility is that polymer contracts in poor solvents, thereby exposing a core-core van der Waals attraction [83]. A second possibility is that polymers contract and a shell-shell van der Waals attraction develops [84]. Perhaps related to this are polymer-polymer interactions [85, 86, 87]. A third possibility is that the polymer undergoes a phase transition to a crystalline state that results in a strong attraction [88].

The PEG-grafted fluorinated particles developed as part of this thesis interact only very weakly, if at all, via core-core van der Waals interactions. In addition, PEG dissolved in ethanol is known to crystallize [89] and provided PEG grafted on particles behave the same way, several of the mechanisms behind attractions between polymer-grafted particles proposed in the literature can be tested.

CHAPTER 5

SUMMARY OF PAPERS

Paper I

In paper I, we employed a semi-batch emulsion polymerization and optimized the synthesis protocol to produce aqueous dispersions of fluorinated spheres without and with a polymer graft. The former has been achieved in the past by others [44, 46] but the latter has proven difficult [51] and quite complicated synthesis routes have been suggested [39]. The present method results in core-shell particles which were thoroughly characterized to ensure that they fulfill a number of requirements usually expected for models system.

For colloidal model systems it is essential to be able to refractive index match the particles and the solvent because it enables the use of optical and light scattering techniques and allows for some control of the van der Waals interaction. However, most existing colloidal model systems consist of particles made of high-refractive-index materials, which limits them to nonaqueous media due to the low refractive index of water. One way to circumvent this problem is to use fluorinated particles. To this end, charged fluorinated spheres have been used to study, e.g., translational and rotational dynamics [90, 91, 92] as well as effects of interactions on the static structure factor [93]. Furthermore, fluorinated latices have served as a host suspension when studying self-diffusion using dynamic light scattering [94]. These bare charged spheres are limited to studying effects of repulsive interactions. When also attractions act between particles, a host of additional phenomena are encountered, such as fluid-fluid phase separation, aggregation, and gel formation.

To be able to carefully pinpoint locations of phase boundaries, the colloidal system should preferably aggregate reversibly. This can be achieved by attaching a polymer at high grafting density onto the fluorinated particles. For this purpose we used methoxy poly(ethylene glycol) acrylate (mPEGA), with a molecular weight (MW) of 2000 g/mol. We chose to evaluate the reversibility of the aggregation using

Na_2CO_3 as an electrolyte since it is known to destabilize PEGylated spheres [95] and free PEG [96]. The grafted spheres show long-term stability in 0.5 M Na_2CO_3, but aggregate in 0.6 M Na_2CO_3. The reversibility of the aggregation is readily confirmed by diluting the aggregated sample such that a salt concentration of 0.5 M Na_2CO_3 is recovered.

The low refractive index of the PEG-grafted particles was confirmed using UV-vis spectroscopy at three different wavelengths. No wavelength dependence was found and the particle refractive index has been determined as 1.384, which can easily be matched in an aqueous solution by adding a cosolvent.

Advantages of particles with low polydispersities are numerous. Dispersions of monodisperse particles are not only convenient for testing theories, but their properties can also be compared with computer simulations of models and the interpretation of scattering data is simplified to a great extent. Furthermore, crystalline phases are absent in polydisperse suspensions [24] and many applications rely on the ability to generate crystalline order [97, 98, 99]. Latices with polydispersities as low as ∼3 %, as determined by SAXS modeling, can be produced with the semi-batch synthesis method provided the molar ratio is kept around 0.05 for these PEG2000-grafted particles.

Finally, to image the particles we have employed cryo-TEM imaging. Bare fluorinated charged spheres in contact can be seen on the left in Fig. 5.1, whereas the image on the right shows PEGylated spheres close to contact.

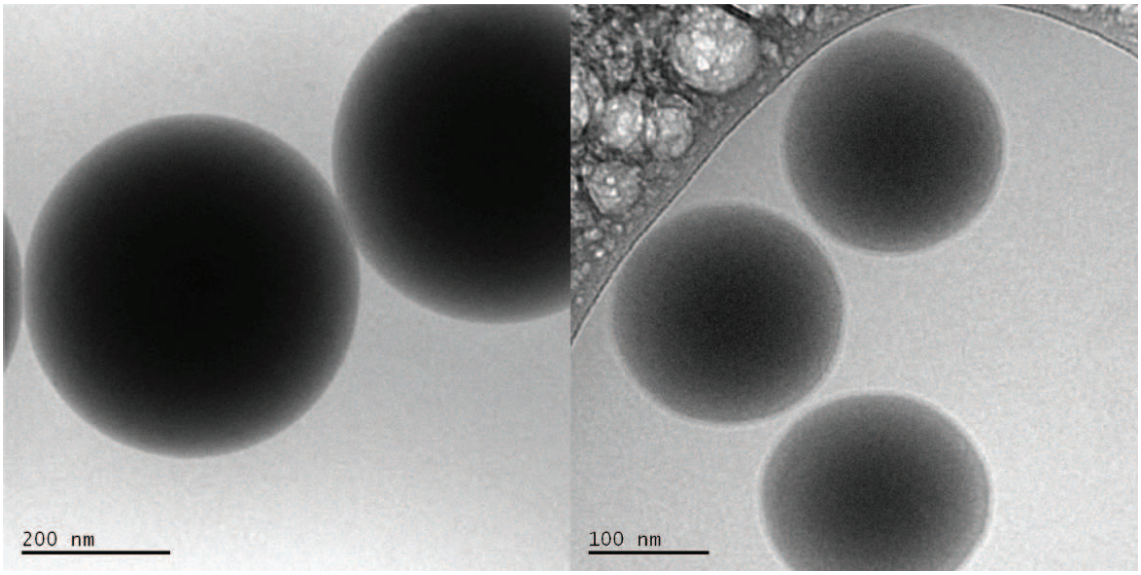

Figure 5.1: Cryo-TEM images of bare charged fluorinated particles (left) and PEGylated fluorinated particles (right).

The PEG-layer is seen as a halo around the particles. Note that the cores in this

case cannot come in intimate contact due to the grafted layer.

Paper II

We investigate the wider applicability of the semi-batch emulsion polymerization developed in Paper I, by grafting both longer (MW 5000 g/mol) and shorter (MW 480 g/mol) PEG chains onto fluorinated particles. To optimize the synthesis, we varied the molar ratio between the PEG macromonomer and the fluorinated monomer. Furthermore, we tested the semi-batch approach on polystyrene latices with a PEG-graft and compared it to a corresponding batch polymerization, with the conclusion that the semi-batch approach results in a more monodisperse size distribution. For the batches with the shorter PEG-grafts, the particle size is relatively unaffected by the molar ratio as long as it is kept below 0.2. The yield increases with increasing molar ratio, but the size distribution develops a tail toward smaller particle sizes as the molar ratio is increased. In Fig. 5.2, the scattering intensity as a function of q is shown for three dispersions synthesized at three different molar ratios, where the solid lines are the fitted form factors. About ten well-defined minima are observed for the dispersions with the lowest molar ratio, whereas the oscillations are less pronounced for the dispersions synthesized with larger molar ratios.

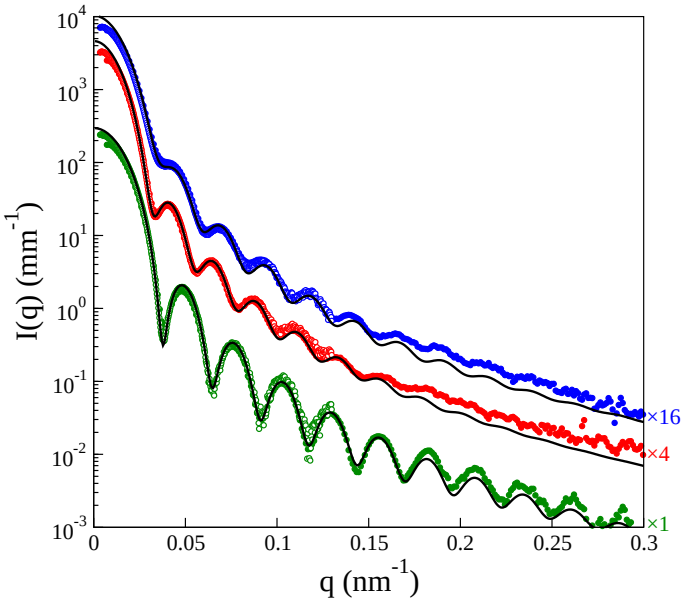

Figure 5.2: Scattering intensity as a function of q for three different dilute dispersions of fluorinated latices with short PEG-grafts. The results have been shifted vertically for clarity as labeled. The open symbols are data recorded with a sample-to-detector distance of 20 m, whereas filled symbols are data recorded at 10 m. The solid lines are fitted form factors.

The variation in molar ratio for the syntheses with PEG5000 also resulted in an increase in yield with increasing molar ratio, although the difference is modest. The

particle size decreases with increasing molar ratio, which is not observed for dispersions synthesized with shorter PEG grafts. In addition, no tail in the size distribution is observed at higher molar ratios with these longer grafts. The scattered intensity as a function of q is shown in Fig. 5.3 for three different molar ratios. The most well-resolved minima are observed for the dispersion with the intermediate molar ratio. However, since the SAXS measurements in Fig. 5.3 were recorded using a laboratory-scale instrument, instrumental resolution effects become more significant the larger the particle size (see Paper III) and it is actually the dispersion made with the lowest molar ratio that has the lowest polydispersity. It is also worthwhile to note that for the PEG5000 dispersions the molar ratio was varied between 0.01-0.045 whereas the corresponding range for the PEG480 dispersions was 0.05-0.2.

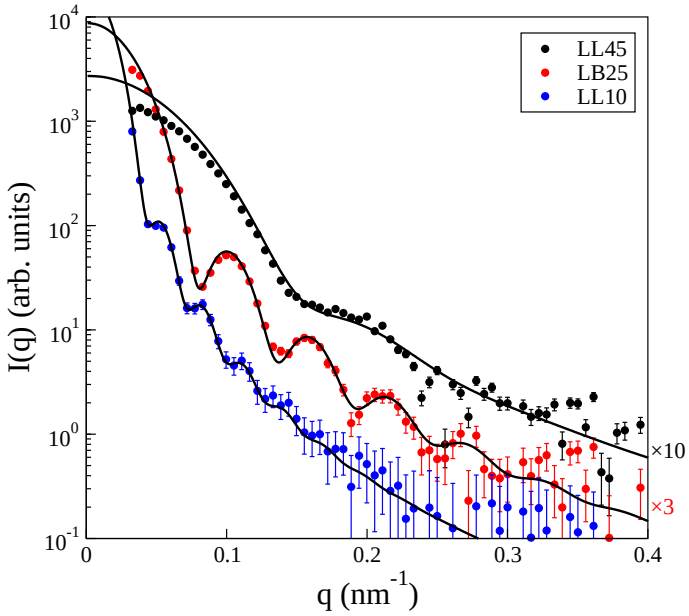

Figure 5.3: Scattering intensity as a function of q for three different dilute dispersions of fluorinated particles bearing long PEG-grafts. The results have been shifted vertically for clarity as labeled. The solid lines are fitted form factors.

The thickness of the PEG-layer (determined as the difference between the hydrodynamic radius and the radius obtained in the SAXS modeling) is roughly 2 nm for the shorter PEG480 graft and between 7-10 nm for the PEG5000 graft. Despite the steric stabilizing layer being only 2 nm for PEG480 dispersions, they show long-term stability in as much as 1 M Na_2CO_3. Fluorinated particles grafted with PEG2000 [100] lose their stability in the range 0.6-0.7 M Na_2CO_3 and for similar particles with PEG5000 the stability limited is found between 0.5-0.6 M Na_2CO_3. The enhanced colloidal stability as the PEG-graft becomes shorter follows the behavior of free PEG solutions [101, 102, 103, 104]. Low molecular weight PEG phase separates at higher salt concentrations. Since the dispersion stability is enhanced using shorter PEG

grafts, the attraction mainly originates from the grafted polymer and is not caused by core-core van der Waals interactions.

Paper III

SAXS is a widely used technique well suited to obtaining structural information about colloids and polymers. However, instrumental smearing effects cannot always be neglected when interpreting scattering data. For synchrotron based radiation, beams are often well collimated and smearing effects due to collimation are minimized. However, for many laboratory-scale SAXS setups, beam collimation is sacrificed in order to increase the radiation flux. Therefore, an efficient way of taking smearing effects into account is called for. This is often done by calculating [105, 106, 107, 108, 109] or simulating [109, 110, 111, 112, 113] the beam profile based on the geometry of the collimation system. Following this, the beam profile is mapped onto a Gaussian profile because the smearing calculation is done more easily for Gaussian profiles [114]. In some cases beam profiles can be measured rather than estimated. For those cases it would be preferable to incorporate the measured beam profile directly in the smearing calculation. This is the approach taken in this work where also an efficient algorithm to accomplish this has been suggested.

We have used fairly monodisperse particles to evaluate instrumental smearing effects on scattering obtained on a laboratory-scale SAXS setup. Fluorinated particles with a core-shell morphology were used because the shell contrast is poor and can be neglected. The rationale for using fluorinated latices, besides the fact that they can be synthesized with a narrow size distribution [71], is their high electron density which gives high contrast in SAXS measurements.

The measured beam profiles of a number of different instrumental configurations are shown in Fig. 5.4. They have been fitted to a suitable function to provide a smooth description of the profiles. An algorithm that allows for rapid direct integration in polar coordinates has been suggested, which has the benefit that any beam profile can be incorporated in smearing calculations. Rather than attempting to desmear experimental data, the algorithm is applied to smear the model intensity.

The smearing effect is illustrated in Fig. 5.5 for three of the different beam profiles in Fig. 5.4. Configuration 26 in Fig. 5.4 has $\sim$50 times higher flux compared to configuration 4, but the data are so smeared that the form factor oscillations are barely visible even though the particles are quite monodisperse. Nonetheless, excellent fits to all the data are obtained (solid lines) with the same set of parameters, a particle radius of 93.8 nm and a polydispersity of 3.8%. This demonstrates that as long as smearing effects are handled accurately even scattering data that are significantly smeared can be usefully modeled.

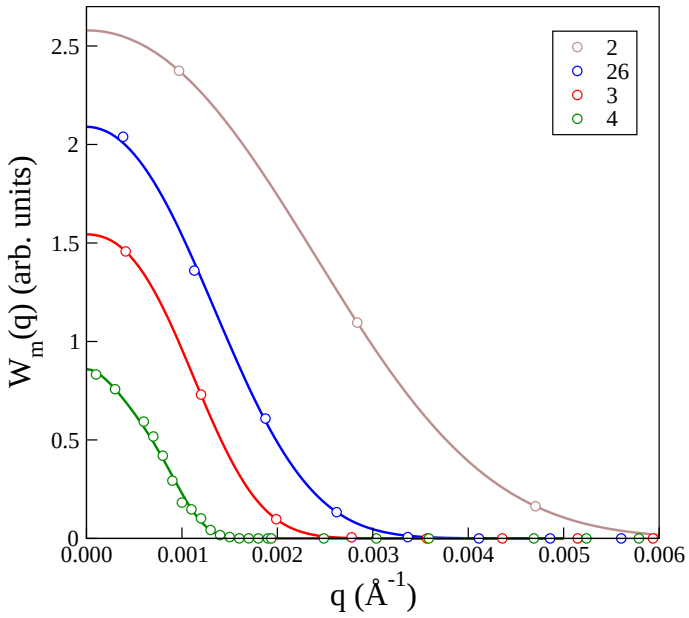

Figure 5.4: Experimentally measured beam profiles versus magnitude of the scattering vector. The solid lines are least-square fits.

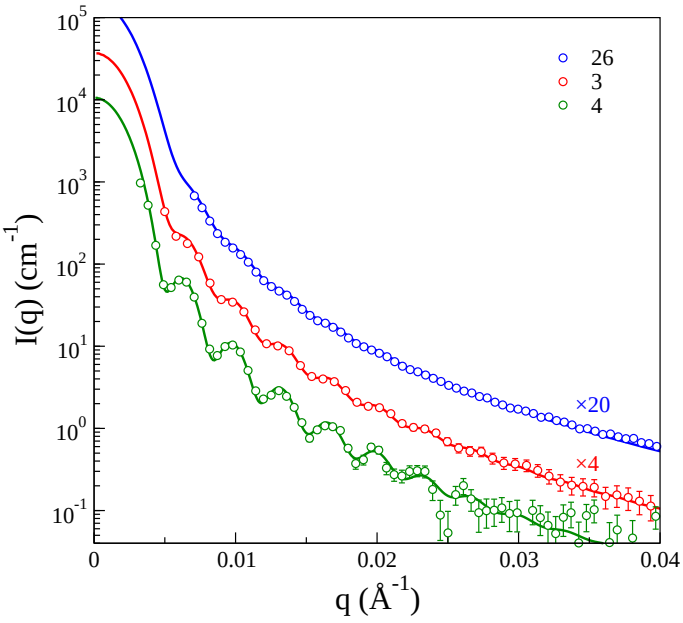

Figure 5.5: Scattering intensity on absolute scale as a function of the scattering vector for PEG-grafted pHFBMA spheres at various configurations of the instrument, as labeled. The solid lines are model form factors, with smearing included using the measured beam profiles. The results have been shifted vertically for clarity as labeled.

Paper IV

Although steric stabilization is robust for well-covered particles, attractions can be induced by adding electrolyte, changing temperature or adding non-adsorbing polymer. The depletion mechanism leads to attractions in the latter case, but the causes of attractions in the two former cases remain unclear. One view is that upon worsening the solvent quality, the polymer layer collapses and exposes a core-core van der Waals force [115, 116, 83]. A second view is that polymer-polymer interactions leads to an attraction [117, 118, 119, 86, 84]. In addition, experiments have revealed polymer crystallization on colloidal surfaces, leading to macroscopic gelation [120, 88, 121]. In this work we use a colloidal model system consisting of fluorinated colloids with grafted PEG-chains. This model system can be used in both aqueous and non-aqueous media, which is exploited here to probe the destabilization mechanism.

Using cryo-TEM, SAXS and DLS, we have investigated the microstructure and the phase behavior under both good and poor solvent conditions for PEG. The solvent quality is worsened either by adding Na_2CO_3 or using ethanol. Free PEG in known to crystallize in ethanol at room temperature [89], so we have replaced the aqueous solution with ethanol as a means to induce attraction. Despite that the core-core van der Waals force is weaker in ethanol compared to water, the attraction is strong enough in ethanol to form fractal structures which was observed in SAXS (data not shown).

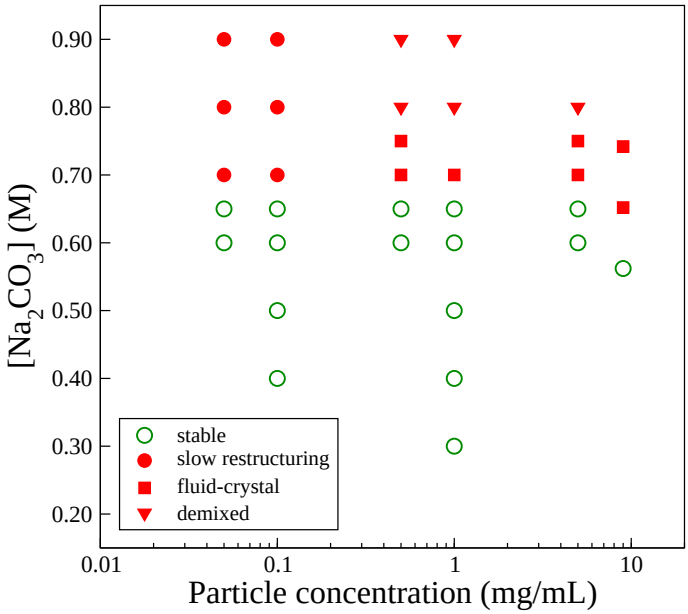

Figure 5.6: Phase behavior of PEG-grafted fluorinated spheres suspended in Na_2CO_3 solutions.

The phase behavior under dilute particle concentrations have been investigated using DLS in Fig. 5.6. Four different regions can be distinguished. At low salt concentrations there is a stable phase which shows long-term stability. Above 0.65 Na_2CO_3 a fluid-crystal coexistence region can be identified when the particle concentration is not too dilute, >0.1 mg/mL, through the presence of crystallites. Below this concentration the dispersion is so dilute so that it is difficult to determine whether crystallites or aggregates form. The formation kinetics is also very slow, which is the reason for labeling this region as 'slowly restructuring'. In the so-called demixed state, at high salt concentrations, particles avoid the solvent either by settling or by positioning themselves at the surface.

The behavior observed resembles what has been reported in depletion systems at low particle concentration [122, 123]. However, the fluid-crystal boundary above the stable region shows an upturn at low particle concentrations in the depletion systems whereas the corresponding boundary is quite flat in Fig. 5.6. Using temperature to induce attractions, Napper et al. [124] observed a flat critical flocculation boundary for PEGylated spheres, whereas Vincent et.al [56, 125] observed an upturn. The difference was attributed to differences in PEG-layer thickness and the magnitude of the induced attractions [125]. Our interpretation is that either the slowly evolving growth process at dilute particle concentrations has gone unnoticed or that the entire stability limit in Fig. 5.6 is a fluid-crystal transition. Furthermore, while preparing these samples, we observed (except for the lowest concentrations) that when a suspension is subjected to a concentrated stock solution of Na_2CO_3, clusters are initially formed that break up within a time frame of a few hours. In other words, the equilibrium behavior is preceded by non-equilibrium effects which make determination of the phase behavior difficult.

We have used SAXS as a means to quantify the interaction as a function of Na_2CO_3 concentration using an adhesive sphere model. SAXS measurements on the same PEG-grafted fluorinated spheres in Paper II have shown that the PEG-layer does not need to be incorporated when modeling form factors [71]. However, it cannot be neglected when evaluating structure factors. Therefore, we have applied cryo-TEM imaging to estimate the PEG-layer thickness at different Na_2CO_3 concentrations, the results of which show that the layer contracts in a gradual manner as the salt concentration is increased.

In modeling the scattering intensities as a function of Na_2CO_3 concentration only the stickiness-parameter of the adhesive sphere model, τ, remains as a fitting parameter. In Fig. 5.7, the fitted SAXS scattering curves are shown as a function of the scattering vector at different salt concentrations for a constant particle concentration. The upturn at low q at 0.54 M demonstrates the presence of clusters that slowly disperse as seen in the inset to Fig. 5.7. The result of the modeling is that the attraction is gradually increasing with increasing amount of salt, which

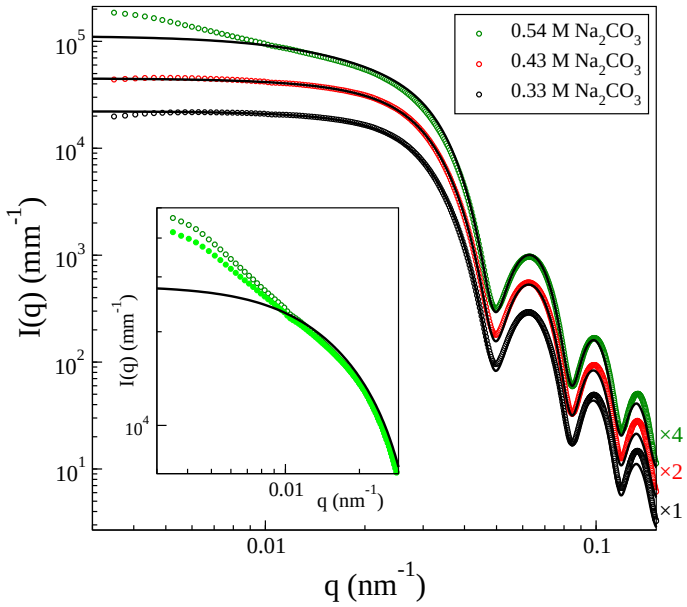

Figure 5.7: Scattering intensity as a function of q for 13 wt% suspension with various amounts of Na_2CO_3, as labeled. The solid lines are the fits according to the adhesive sphere model. The results have been shifted vertically for clarity as labeled. The inset shows the intensity at a Na_2CO_3 concentration of 0.54 M decreases with time, where the intensity has been recorded with a 30 min time interval.

follows the gradual contraction of the PEG graft. This behavior is in agreement with computer simulations of pair interactions between polymer-grafted spheres [87]. In contrast, similar measurements on particles dispersed in ethanol show that fractal aggregation occurs, from which one can infer strong attractions between particles. As demonstrated in Paper II the origin of these attractions is not core-core van der Waals interactions. Instead, they are caused by the grafted PEG. We speculate that the reason for the far stronger attractions in ethanol is that the PEG chains crystallize, whereas in aqueous systems they adopt a more compact structure to avoid contact with the solvent.

CHAPTER 6

CONCLUSIONS AND OUTLOOK

Although colloidal model system have proven very useful in studying phenomena in colloid science and condensed matter physics, they have been limited for the most part to nonaqueous media. Therefore, aqueous colloidal model systems are called for. We have devised a synthesis route to produce monodisperse fluorinated latices bearing a PEGylated graft. The high degree of monodispersity, the low refractive index of the fluorinated core polymer, and the PEG-graft make them suitable as model sterically stabilized systems.

The particles were synthesized using a semi-batch emulsion polymerization, where the initiator was fed slowly into the reaction mixture. Slow feeding of the initiator has been used previously in homo-polymerization, but its applicability in the preparation of core-shell particles through co-polymerization has not been evaluated.

Several properties such as colloidal stability [126] and optical properties [127] are related to the properties of the stabilizing layer, such as grafting density and thickness. This together with a wish to test the wider applicability of the semi-batch approach served as a motivation for grafting polymers of various length onto fluorinated spheres. Particles grafted with PEG480 and PEG5000 were successfully synthesized in addition to the ones with grafted PEG2000. The molar ratio of the PEG macromonomer to the fluorinated monomer was shown to influence the size distribution strongly. The synthesis procedure was also shown to lower the polydispersity of polystyrene particles with a PEGylated graft.

In applications of this model system, we have mapped out the low-concentration part of the phase diagram for these sterically stabilized colloids exposed to high concentrations of sodium carbonate. The salt serves to decrease the solvent quality for the PEG graft. In these dilute systems particles tend to form crystals due to attractions between particles. The attractions are not caused by the usual van

der Waals interaction between homogeneous particles. Instead, it was shown to be caused by interactions mediated by the PEG grafts because the particle stability was shown to increase as the length of the PEG graft was decreased. For systems dominated by a core-core van der Waals interaction the opposite trend should follow. Using cryo-TEM and SAXS it was shown that the addition of salt leads to a gradual compaction of the PEG graft and the development of a weak to modest attraction. In contrast, dispersing the particles in ethanol leads to much stronger attractions, which are presumably caused by freezing of the PEG chains.

In terms of future extension of this work, access to higher particle concentrations would be required to enable studies of rheology and more complete studies of the phase behavior. For this the synthesis would need to be scaled up. In addition, based on the aggregation of these particles that occurs in ethanol, it would be interesting to investigate colloidal stability in various solvents. This would serve as further probe of the influence of the PEG graft on interactions between particles. In this context, we have developed and evaluated a simple and fast method based on centrifugation to replace the aqueous solution with simple alcohols. Although no swelling was observed in ethanol, we note that cross-linking of the fluorinated polymer might be required to avoid swelling in other solvents.

Studies have claimed that there is an equivalence with regard to interparticle attractions induced by increasing temperature and by increasing salt concentrations [128]. Previous studies on PEGylated polystyrene spheres showed that in the presence of appreciably amount Na_2CO_3, temperature could indeed be used to increase the attraction further [73]. However, for these sterically stabilized fluorinated latices, no temperature dependence of the phase boundary was observed in an interval between 5-40 °C. This seeming contradiction calls for further studies.

Most of the focus in terms of the synthesis procedure was to produce monodisperse core-shell particles, and little emphasis was given to changing particle size. One possible way to control particle radius (which never was tested) is to change the monomer/water ratio in the synthesis. If the particles were smaller, studies of the interactions would be much simpler. For instance, DLS measurements would yield the collective diffusion coefficient which is sensitive to interactions between particles. Also, the structure factor peak would be shifted to lower q for smaller particles, so that a laboratory-scale SAXS instrument would be sufficient for observing effects of interactions. Also, if the particles were larger (and fluorescently labeled), confocal microscopy can be used to study real-time collective behavior. Simultaneous refractive index matching and density matching can be achieved by adding a mixture of salt to water or using a mixture of solvents [129].

The grafting density plays a key role in colloidal stability. In the work presented in this thesis the grafting density was not quantified. In other words, it is not

known whether the grafting density changes significantly when PEG chains of various length are grafted on the particles. There is a need for a reliable method to determine grafting density that works also for densely grafted systems.

We were able to observe a contraction of the PEG-layer with increasing amount of salt using cryo-TEM imaging. However, little is known about the polymer dynamics as solvent quality is worsened in colloidal suspensions. The studies have so far been limited to adsorbed [130] and polydisperse [131] grafted planar surfaces in organic solvents. In aqueous solutions, studies have been restricted to planar surfaces at low grafting densities [132]. In a non-aqueous colloidal suspension of silica, Roke et.al. were able to observe grafted hydrocarbon chains crossing over from a liquid-like morphology to crystalline order as the colloids went from stable to their gelled state upon lowering the temperature [88]. A similar structural transition is suspected to be responsible for the aggregation that occurs when the PEG-grafted particles studied in this work are transferred to ethanol. One would expect a dramatic change in the dynamics of the grafted polymer in connection with this structural transition. Attempts to capture the PEG-polymer dynamics with DLS by canceling out the core scattering through contrast matching proved unsuccessful due in part to density fluctuations of the solvent mixture. This polymer dynamics, which occurs on small length and time scales, can be studied using neutron spin echo, studies which could lead to an increase of our understanding of the relation between microscopic and macroscopic properties.

ACKNOWLEDGEMENTS

Johan Bergenholtz: A special thanks for enrolling me on this journey. We have had many interesting discussions about various phenomena and literature which I really enjoyed. Thank you for always being understanding, supportive and for always being open-minded to all my (sometimes crazy) ideas.
Kristin Jonsson: Welcome to our small research group! I cannot think of a better person to continue moving this project forward.
Elisabet Ahlberg: Thank you for taking on the role as examiner and for making sure that the work progressed as planned.
Zareen Abbas: Thank you for co-supervising this project.
Anna Reymer: My former office-roommate and dear friend who always had a good advice to share about all aspects of life.
Sandra Rocha: For all your support and advice.
Gunnel Karlsson: For all cryo-TEM expertise.
Jenny Bergman: Thank you for sharing the "teaching workload" and for being a wonderful office-roommate. You, being my antipole sure made me question several aspects of life.
Jenny P.H: For always having a smile on your face and a good advice or two to share.
Moheb Nayeri: For welcoming me into the lab and showing me around.
Karin Danielsson: Together we explored the colloidal domain and much more!
Monika Witala: For all our discussions and laughters.
Julian Gallego, Geert Cornelis: For letting me make a lot of noise on the 4th floor.
Andrea Borchini: Thanks for the lunch discussions we had. I have sure learned a lot about Italy.
Malin Zackrisson Oskolkova: We sure experienced some mind blowing experiments together!
Staffan Wall: Thank you for inviting me into your private library.
Åke Nilsson: Although organic chemistry never was my cup of tea, I never would have considered taking a PhD if it wasn't for you!

The "Lunch-crew" (past and present): Although my attendance has been low for the last couple of months, I sure enjoyed all our discussions.
The Electro-chemistry group: Thank you for taking on a colloidal chemist.
The Physical-chemistry group: For all our topics we have debated over the years.
My family: For supporting me on this journey in so many ways!
My son, Kevin: My greatest inspiration in life. Thank you for your support and understanding. Thank you for always believing in me, it is enormously cherished.

BIBLIOGRAPHY

[1] J. G. Riess. Blood substitutes and other potential biomedical applications of fluorinated colloids. *J. Fluorine Chem.*, 114:119 – 126, 2002.

[2] R. J. Hunter. *Introduction to Modern Colloid Science*. Oxford University Press, 1993.

[3] P. J. Lu and D. A. Weitz. Colloidal Particles: Crystals, Glasses, and Gels. *Annu. Rev. Condens. Matter Phys.*, 4:217–233, 2013.

[4] C. D. Andersson and E. S. Daniels. *Emulsion polymerisation and latex applications*, volume 14 of *Rapra review reports. Report 160,*. Rapra Technology Smithers Rapra Press, 2003.

[5] P. N. Pusey and W. van Megen. Phase behaviour of concentrated suspensions of nearly hard colloidal spheres. *Nature*, 320:340–342, 1986.

[6] L. Antl, J. W. Goodwin, R. D. Hill, R. H. Ottewill, S. M. Owens, S. Papworth, and J. A. Waters. The preparation of poly(methyl methacrylate) latices in non-aqueous media. *Colloids Surf.*, 17:67 – 78, 1986.

[7] P. N. Pusey, W. Van Megen, S. M. Underwood, P. Bartlett, and R. H. Ottewill. Colloidal fluids, crystals and glasses. *Physica A*, 176:16 – 27, 1991.

[8] A. K. Van Helden, J. W. Jansen, and A. Vrij. Preparation and characterization of spherical monodisperse silica dispersions in nonaqueous solvents . *J. Colloid. Interf. Sci.*, 81:354 – 368, 1981.

[9] B. R. Saunders and B. Vincent. Microgel particles as model colloids: theory, properties and applications. *Adv. Colloid Interf. Sci.*, 80:1 – 25, 1999.

[10] K. N. Pham, A. M. Puertas, J. Bergenholtz, S. U. Egelhaaf, A. Moussaïd, P. N. Pusey, A. B. Schofield, M. E. Cates, M. Fuchs, and W. C. K. Poon. Multiple glassy states in a simple model system. *Science*, 296:104–106, 2002.

[11] J. Mattsson, H. M. Wyss, A. Fernandez-Nieves, K. Miyazaki, Z. Hu, D. R. Reichman, and D. A. Weitz. Soft colloids make strong glasses. *Nature*, 462:83–86, 2009.

[12] P. N. Pusey and W. van Megen. Observation of a glass transition in suspensions of spherical colloidal particles. *Phys. Rev. Lett.*, 59:2083–2086, 1987.

[13] S. M. Ilett, A. Orroc, W. C. K. Poon, and P. N. Pusey. Phase behavior of a model colloid-polymer mixture. *Phys. Rev. E*, 51:1344–1352, 1995.

[14] C. P. Lowe and D. Frenkel. Short-time dynamics of colloidal suspensions. *Phys. Rev. E*, 54:2704–2713, 1996.

[15] A. J. Banchio, J. Bergenholtz, and G. Nägele. Rheology and dynamics of colloidal suspensions. *Phys. Rev. Lett.*, 82:1792–1795, 1999.

[16] G. Nägele, B. Steininger, U. Genz, and R. Klein. Short-time dynamics of charge-stabilized colloidal suspensions. *Physica Scripta*, 1994:119, 1994.

[17] P. N. Segrè and P. N. Pusey. Scaling of the dynamic scattering function of concentrated colloidal suspensions. *Phys. Rev. Lett.*, 77:771–774, 1996.

[18] P. Holmqvist and G. Nägele. Long-time dynamics of concentrated charge-stabilized colloids. *Phys. Rev. Lett.*, 104:058301, 2010.

[19] A. Kasper, E. Bartsch, and H. Sillescu. Self-Diffusion in concentrated colloid suspensions studied by digital video microscopy of core-shell tracer particles. *Langmuir*, 14:5004–5010, 1998.

[20] U. Gasser, E. R. Weeks, A. Schofield, P. N. Pusey, and D. A. Weitz. Real-space imaging of nucleation and growth in colloidal crystallization. *Science*, 292:258–262, 2001.

[21] D. J. W. Aastuen, N. A. Clark, L. K. Cotter, and B. J. Ackerson. Nucleation and growth of colloidal crystals. *Phys. Rev. Lett.*, 57:1733–1736, 1986.

[22] J. K. G. Dhont, C. Smits, and H. N. W. Lekkerkerker. A time resolved static light scattering study on nucleation and crystallization in a colloidal system. *J. Colloid. Interf. Sci.*, 152:386 – 401, 1992.

[23] J. L. Harland and W. van Megen. Crystallization kinetics of suspensions of hard colloidal spheres. *Phys. Rev. E*, 55:3054–3067, 1997.

[24] S. M. Liddle, T. Narayanan, and W. C. K. Poon. Polydispersity effects in colloid-polymer mixtures. *J. Phys.: Condens. Matter*, 23:194116, 2011.

[25] A. Yethiraj. Tunable colloids: control of colloidal phase transitions with tunable interactions. *Soft Matter*, 3:1099–1115, 2007.

[26] D. A. Weitz and M. Oliveria. Fractal structures formed by kinetic aggregation of aqueous gold colloids. *Phys. Rev. Lett.*, 52:1433–1436, 1984.

[27] M. Y. Lin, H. M. Lindsay, D. A. Weitz, R. C. Ball, R. Klein, and P. Meakin. Universality in colloid aggregation. *Nature*, 339:360–362, 1989.

[28] H. Verduin and J. K. G. Dhont. Phase diagram of a model adhesive hard-sphere dispersion. *J. Colloid. Interf. Sci.*, 172:425 – 437, 1995.

[29] J. Bergenholtz, W. C. K. Poon, and M. Fuchs. Gelation in model colloid-polymer mixtures. *Langmuir*, 19:4493–4503, 2003.

[30] E. Zaccarelli. Colloidal gels: equilibrium and non-equilibrium routes. *J. Phys.: Condens. Matter*, 19:323101, 2007.

[31] J. C. van der Werff and C. G. de Kruif. Hard sphere colloidal dispersions: The scaling of rheological properties with particle size, volume fraction, and shear rate. *J. Rheol.*, 33:421–454, 1989.

[32] M. Fuchs and M. Ballauff. Flow curves of dense colloidal dispersions: Schematic model analysis of the shear-dependent viscosity near the colloidal glass transition. *J. Chem. Phys.*, 122:–, 2005.

[33] R. G. Gilbert. *Emulsion polymerization.* Academic press, 1995.

[34] M. Hoffmann, Y. Lu, M. Schrinner, M. Ballauff, and L. Harnau. Dumbbell-shaped polyelectrolyte brushes studied by depolarized dynamic light scattering. *J. Phys. Chem. B*, 112:14843–14850, 2008.

[35] P. M. Johnson, C. M. van Kats, and A. van Blaaderen. Synthesis of colloidal silica dumbbells. *Langmuir*, 21:11510–11517, 2005.

[36] T. Nisisako, T. Torii, T. Takahashi, and Y. Takizawa. Synthesis of monodisperse bicolored janus particles with electrical anisotropy using a microfluidic co-flow system. *Adv. Mat.*, 18:1152–1156, 2006.

[37] B. Liu, H. Mohwald, and D. Wang. Synthesis of Janus particles via kinetic control of phase separation in emulsion droplets. *Chem. Commun.*, 49:9746–9748, 2013.

[38] G. Zhang and X. W. D. Lou. General synthesis of multi-shelled mixed metal oxide hollow spheres with superior lithium storage properties. *Angewandte Chemie International Edition*, 53:9041–9044, 2014.

[39] D. Burger, J. Gisin, and E. Bartsch. Synthesis of sterically stabilized perfluorinated aqueous latices. *Colloids Surf. A*, 442:123 – 131, 2014.

[40] J. W. Jansen, C. G. de Kruif, and A. Vrij. Attractions in sterically stabilized silica dispersions: II. Experiments on phase separation induced by temperature variation. *J. Colloid. Interf. Sci.*, 114:481 – 491, 1986.

[41] W. V. Smith and R. H. Ewart. Kinetics of emulsion polymerization. *J. Chem. Phys.*, 16:592–599, 1948.

[42] R. M. Fitch and C. H. Tsai. Particle formation in polymer colloids, III: Prediction of the number of particles by a homogeneous nucleation theory. In R. M. Fitch, editor, *Polymer Colloids*, pages 73–102. Springer US, 1971.

[43] J. Ugelstad and F. K. Hansen. Kinetics and mechanism of emulsion polymerization. *Rubber Chem. Technol.*, 49:536–609, 1976.

[44] W. Härtl and X. Zhang-Heider. The synthesis of a new class of polymer colloids with a low index of refraction. *J. Colloid. Interf. Sci.*, 185:398–401, 1997.

[45] G. Pan, A. S. Tse, R. Kesavamoorthy, and S. A. Asher. Synthesis of highly fluorinated monodisperse colloids for low refractive index crystalline colloidal arrays. *J. American Chem. Soc.*, 120:6518–6524, 1998.

[46] G. H. Koenderink, S. Sacanna, C. Pathmamanoharan, M. Raşa, and A. P. Philipse. Preparation and properties of optically transparent aqueous dispersions of monodisperse fluorinated colloids. *Langmuir*, 17:6086–6093, 2001.

[47] G. H. Koenderink S. Sacanna and A. P. Philipse. Microemulsion synthesis of fluorinated latex spheres. *Langmuir*, 20:8398–8400, 2004.

[48] C. W. A. Bromley. The preparation of sterically stabilised aqueous latices using polyethylene oxide. *Colloids Surf.*, 17:1–11, 1986.

[49] R. H. Ottewill and R. Satgurunathan. Nonionic latices in aqueous media part 1. Preparation and characterization of polystyrene latices. *Colloid Polym. Sci.*, 265:845–853, 1987.

[50] A. Brindley, S. S. Davis, M. C. Davies, and J. F. Watts. Polystyrene colloids with surface-grafted polyethylene oxide as model systems for site-specific drug delivery: I. Preparation and surface chemical characterization using SIMS and XPS. *J. Colloid. Interf. Sci.*, 171:150 – 161, 1995.

[51] M. Wiemann, R. Schneider, and E. Bartsch. Synthesis of PEG-stabilized fluoro-acrylate particles and study of their glass transition in aqueous dispersion. *Zeitschrift für Physikalische Chemie*, 226:761–778, 2012.

[52] Z. Luo, C. Zou, S. Syed, L. A. Syarbaini, and G. Chen. Highly monodisperse chemically reactive sub-micrometer particles: polymer colloidal photonic crystals. *Colloid Polym. Sci.*, 290:141–150, 2012.

[53] R. N. Madan and R. C. Dikshit. Effect of various modes of initiator addition on semicontinuous copolymerization of styrene-butylacrylate. *Indian J. Chem. Technol.*, 11:74–79, 2004.

[54] H. C. Lichstein and M. H. Soule. Studies of the effect of sodium azide on microbic growth and respiration: I. the action of sodium azide on microbic growth. *J. Bact.*, 47:221–230, 1944.

[55] G. Fritz, V. Schädler, N. Willenbacher, and N. J. Wagner. Electrosteric stabilization of colloidal dispersions. *Langmuir*, 18:6381–6390, 2002.

[56] C. Cowell, R. Li-In-On, and B. Vincent. Reversible flocculation of sterically-stabilised dispersions. *J. Chem. Soc., Faraday Trans. 1*, 74:337–347, 1978.

[57] P. J. Roth, M. Collin, and C. Boyer. Advancing the boundary of insolubility of non-linear PEG-analogues in alcohols: UCST transitions in ethanol-water mixtures. *Soft Matter*, 9:1825–1834, 2013.

[58] J. K. G. Dhont. *An Introduction to Dynamics of Colloids*. Studies in Interface Science Vol.2, Elsevier Science B.V, 1996.

[59] Pusey et.al. *Neutrons, X-rays and Light: Scattering Methods Applied to Soft Condensed Matter*. Elsevier Science B.V, 2002.

[60] B. J. Berne and R. Pecora. *Dynamic Light Scattering with Applications to Chemistry, Biology, and Physics*. Dover publications, 2000.

[61] D. E. Koppel. Analysis of Macromolecular Polydispersity in Intensity Correlation Spectroscopy: The Method of Cumulants. *J. Chem. Phys.*, 57:4814–4820, 1972.

[62] J. C. Brown, P. N. Pusey, and R. Dietz. Photon correlation study of polydisperse samples of polystyrene in cyclohexane. *J. Chem. Phys.*, 62:1136, 1975.

[63] D. L. Sidebottom and T. D. Tran. Universal patterns of equilibrium cluster growth in aqueous sugars observed by dynamic light scattering. *Phys. Rev. E*, 82:051904, 2010.

[64] K. Elamin and J. Swenson. Brownian motion of single glycerol molecules in an aqueous solution as studied by dynamic light scattering. *Phys. Rev. E*, 91:032306, 2015.

[65] B. R. Ware and W. H. Flygare. The simultaneous measurement of the electrophoretic mobility and diffusion coefficient in bovine serum albumin solutions by light scattering. *Chem. Phys. Lett.*, 12(1):81 – 85, 1971.

[66] H. Ohshima. *Electrical Phenomena at Interfaces and Biointerfaces*. John Wiley & sons Inc., 2012.

[67] A. K. Varshneya. *Fundamentals of Inorganic Glasses*. Academic Press Inc., 1994.

[68] D. B. Williams and C. B. Carter. *Transmission Electron Microscopy A Textbook for Materials Science*. Plenum Press, 1996.

[69] Disc Centrifuge Operating Manual. *http://www.cpsinstruments.eu/pdf/Manual.pdf*.

[70] D. F. Evans and H. Wennerström. *The colloidal domain*. Wiley-VCH, 1999.

[71] J. Ulama, M. Zackrisson Oskolkova, and J. Bergenholtz. Monodisperse PEGylated spheres: An aqueous colloidal model system. *J. Phys. Chem. B*, 118:2582–2588, 2014.

[72] M. A. Bevan and D. C. Prieve. Forces and hydrodynamic interactions between polystyrene surfaces with adsorbed PEO-PPO-PEO. *Langmuir*, 16:9274–9281, 2000.

[73] M. Zackrisson Oskolkova, A. Stradner, J. Ulama, and J. Bergenholtz. Concentration-dependent effective attractions between PEGylated nanoparticles. *RSC Adv.*, 5:25149–25155, 2015.

[74] H. C. Hamaker. The London-van der Waals attraction between spherical particles. *Physica*, 4:1058 – 1072, 1937.

[75] I. E. Dzyaloshinskii, E. M. Lifshitz, and L. P. Pitaevskii. The general theory of van der Waals forces. *Adv. Phys.*, 10:165–209, 1961.

[76] E. M. Lifshitz. The theory of molecular attractive forces between solids. *Sov. Phys. JETP 2*, 2:73–83, 1956.

[77] J. N. Israelachvili. *Intermolecular and Surface Forces*. Academic Press, New York, 2nd edition, 1991.

[78] J. Mahanty and B. W. Ninham. *Dispersion forces*. London Academic Press, 1976.

[79] A. Yethiraj and A. van Blaaderen. A colloidal model system with an interaction tunable from hard sphere to soft and dipolar. *Nature*, 421:513–517, 2003.

[80] H. Holthoff, S. U. Egelhaaf, M. Borkovec and P. Schurtenberger, and H. Sticher. Coagulation rate measurements of colloidal particles by simultaneous static and dynamic light scattering. *Langmuir*, 12:5541–5549, 1996.

[81] D. H. Napper. *Polymeric stabilization of colloidal dispersions*. Academic Press, London, 1983.

[82] W. B. Russel, D. A. Saville, and W. R. Schowalter. *Colloidal dispersions*. Cambridge, New York, 1989.

[83] R. C. Kramb and C. F. Zukoski. A metastable van der Waals gel: Transitioning from weak to strong attractions. *Langmuir*, 24:7565–7572, 2008.

[84] M. A. Bevan, S. N. Petris, and D. Y. C. Chan. Solvent quality dependent continuum van der Waals attraction and phase behavior for colloids bearing nonuniform adsorbed polymer layers. *Langmuir*, 18:7845–7852, 2002.

[85] P. M. Claesson, R. Kjellander, P. Stenius, and H. K. Christenson. Direct measurement of temperature-dependent interactions between non-ionic surfactant layers. *J. Chem. Soc., Faraday Trans. 1*, 82:2735–2746, 1986.

[86] B. Lemaire, P. Bothorel, and D. Roux. Micellar interactions in water-in-oil microemulsions. 1. Calculated interaction potential. *J. Phys. Chem.*, 87:1023–1028, 1983.

[87] F. LoVerso, S. A. Egorov, and K. Binder. Interaction between polymer brush-coated spherical nanoparticles: Effect of solvent quality. *Macromolecules*, 45:8892–8902, 2012.

[88] S. Roke, O. Berg, J. Buitenhuis, A. van Blaaderen, and M. Bonn. Surface molecular view of colloidal gelation. *Proc. Natl. Acad. Sci.*, 103:13310–13314, 2006.

[89] D. L. Ho, B. Hammouda, S. R. Kline, and W. R. Chen. Unusual phase behavior in mixtures of poly(ethylene oxide) and ethyl alcohol. *J. Polym. Sci. B*, 44:557–564, 2005.

[90] G. H. Koenderink and A. P. Philipse. Rotational and translational self-diffusion in colloidal sphere suspensions and the applicability of generalized Stokes-Einstein relations. *Langmuir*, 16:5631–5638, 2000.

[91] V. Degiorgio, R. Piazza, and T. Bellini. Static and dynamic light scattering study of fluorinated polymer colloids with a crystalline internal structure. *Adv. Colloid Interf. Sci.*, 48:61 – 91, 1994.

[92] V. Degiorgio, R. Piazza, and R. B. Jones. Rotational diffusion in concentrated colloidal dispersions of hard spheres. *Phys. Rev. E*, 52:2707–2717, 1995.

[93] W. Härtl and H. Versmold. Temperature dependence of the structure factor S(Q) of liquid-like ordered colloidal dispersions. *J. Chem. Phys.*, 81:2507–2510, 1984.

[94] W. Härtl, H. Versmold, and X. Zhang-Heider. Tracer particle diffusion in crystal- and fluid-like ordered colloidal suspensions. *Berichte der Bunsengesellschaft für physikalische Chemie*, 95:1105–1111, 1991.

[95] M. Zackrisson, A. Stradner, P. Schurtenberger, and J. Bergenholtz. Small-angle neutron scattering on a core-shell colloidal system: a contrast-variation study. *Langmuir*, 21:10835–10845, 2005.

[96] K. P. Ananthapadmanabhan and E. D. Goddard. Aqueous biphase formation in polyethylene oxide-inorganic salt systems. *Langmuir*, 3:25–31, 1987.

[97] A. Stein, B. E. Wilson, and S. G. Rudisill. Design and functionality of colloidal-crystal-templated materials-chemical applications of inverse opals. *Chem. Soc. Rev.*, 42:2763–2803, 2013.

[98] O.Sato, S. Kubo, and Z-Z. Gu. Structural color films with lotus effects, superhydrophilicity, and tunable stop-bands. *Acc. Chem. Res.*, 42:1–10, 2009.

[99] A. D. Dinsmore, M. F. Hsu, M. G. Nikolaides., M. Marquez, A. R. Bausch, and D. A. Weitz. Colloidosomes: Selectively permeable capsules composed of colloidal particles. *Science*, 298:1006–1009, 2002.

[100] J. Ulama, M. Zackrisson Oskolkova, and J. Bergenholtz. Polymer-graft-mediated interactions between colloidal spheres. *To be published*.

[101] N. Voros, P. Proust, and A. Fredenslund. Liquid-liquid phase equilibria of aqueous two-phase systems containing salts and polyethylene glycol. *Fluid Phase Equilibr.*, 90:333 – 353, 1993.

[102] K. Osseo-Asare and X. Zeng. Partition of pyrite in aqueous biphase systems. *Int. J. Miner. Process.*, 58:319 – 330, 2000.

[103] M. E. Taboada, J. A. Asenjo, and B. A. Andrews. Liquid-liquid and liquid-liquid-solid equilibrium in Na_2CO_3-PEG-H_2O. *Fluid Phase Equilibr.*, 180:273 – 280, 2001.

[104] M. R. Almeida, H. Passos, M. M. Pereira, Á. S. Lima, J. A. P. Coutinho, and M. G. Freire. Ionic liquids as additives to enhance the extraction of antioxidants in aqueous two-phase systems. *Sep. Purif. Technol.*, 128:1 – 10, 2014.

[105] J. A. Miller, S. L. Cooper, C. C. Han, and G. Pruckmayr. Small-angle neutron scattering from a polyurethane block copolymer. *Macromolecules*, 17:1063–1071, 1984.

[106] D. F. R. Mildner and J. M. Carpenter. Optimization of the experimental resolution for small-angle scattering. *J. Appl. Cryst.*, 17:249–256, 1984.

[107] V. Ramakrishnan. A treatment of instrumental smearing effects in circularly symmetric small-angle scattering. *J. Appl. Cryst.*, 18:42–46, 1985.

[108] P. W. Schmidt. Collimation effects in small-angle X-ray and neutron scattering. *J. Appl. Cryst.*, 21:602–612, 1988.

[109] J. S. Pedersen, D. Posselt, and K. Mortensen. Analytical treatment of the resolution function for small-angle scattering. *J. Appl. Cryst.*, 23:321–333, 1990.

[110] B. Lai and F. Cerrina. Shadow: a synchrotron radiation ray tracing program. *Nucl. Instrum. Meth. A*, 246:337–341, 1986.

[111] J. S. Pedersen. Resolution effects and analysis of small-angle neutron scattering data. *J. Phys. IV (Paris)*, 3:491–498, 1993.

[112] P. Harris, B. Lebech, and J. S. Pedersen. The three-dimensional resolution function for small-angle scattering and Laue geometries. *J. Appl. Cryst.*, 28:209–222, 1995.

[113] J. S. Pedersen. A flux- and background-optimized version of the NanoSTAR small-angle X-ray scattering camera for solution scattering. *J. Appl. Cryst.*, 37:369–380, 2004.

[114] J. S. Pedersen, D. Posselt, and K. Mortensen. Analytical treatment of the resolution function for small-angle scattering. *J. Appl. Cryst*, 23:321–333, 1990.

[115] F. Th. Hesselink, A. Vrij, and J. Th. G. Overbeek. On the theory of the stabilization of dispersions by adsorbed macromolecules. II. Interaction between two flat particles. *J. Phys. Chem.*, 75:2094, 1971.

[116] A. K. Dolan and S. F. Edwards. Theory of the stabilization of colloids by adsorbed polymer. *Proc. R. Soc. Lond. A*, 337:509, 1974.

[117] M. J. Vold. The effect of adsorption on the van der Waals interaction of spherical colloidal particles. *J. Colloid. Interf. Sci.*, 16:1–12, 1961.

[118] D. Langbein. Theory of van der Waals attraction. In *Springer Tracts in Modern Physics, No. 72*. Springer-Verlag, New York, 1974.

[119] J. E. Kiefer, V. A. Parsegian, and G. H. Weiss. Model for van der Waals attraction between spherical particles with nonuniform adsorbed polymer. *J. Colloid. Interf. Sci.*, 51:543–546, 1975.

[120] S. Roke, J. Buitenhuis, J. C. van Miltenburg, M. Bonn, and A. van Blaaderen. Interface-solvent effects during colloidal phase transitions. *J. Phys.: Condens. Matter*, 17:S3469, 2005.

[121] A. P. R. Eberle, N. J. Wagner, B. Akgun, and S. K. Satija. Temperature-dependent nanostructure of an end-tethered octadecane brush in tetradecane and nanoparticle phase behavior. *Langmuir*, 26:3003–3007, 2010.

[122] W. C. K. Poon, A. D. Pirie, and P. N. Pusey. Gelation in colloid-polymer mixtures. *Faraday Discuss.*, 101:65–76, 1995.

[123] M. S. Romero-Cano and A. M. Puertas. Phase behaviour of a model colloid-polymer mixture at low colloid concentration. *Soft Matter*, 4:1242–1248, 2008.

[124] R. I. Feigin, J. Dodd, and D. H. Napper. The effects of particle configurational entropy on the flocculation of sterically stabilized dispersions. *Colloid Polym. Sci.*, 259:1027–1030, 1981.

[125] C. Cowell and B. Vincent. Temperature-particle concentration phase diagrams for dispersions of weakly interacting particles. *J. Colloid. Interf. Sci.*, 87:518 – 526, 1982.

[126] K. Ohno. Colloidal crystals formed by polymer brush-afforded fine particles. *Polym. Chem.*, 1:1545–1551, 2010.

[127] S. Magkiriadou, J-G. Park, Y-S. Kim, and V. N. Manoharan. Disordered packings of core-shell particles with angle-independent structural colors. *Opt. Mater. Express*, 2:1343–1352, 2012.

[128] G. E. Fernandes and M. A. Bevan. Equivalent temperature and specific ion effects in macromolecule-coated colloid interactions. *Langmuir*, 23:1500–1506, 2007.

[129] S. Wiederseiner, N. Andreini, G. Epely-Chauvin, and C. Ancey. Refractive-index and density matching in concentrated particle suspensions: a review. *Exp. Fluids*, 50:1183–1206, 2011.

[130] G. Fytas, S. H. Anastasiadis, R. Seghrouchni, D. Vlassopoulos, J. Li, B. J. Factor, W. Theobald, and C. Toprakcioglu. Probing collective motions of terminally anchored polymers. *Science*, 274:2041–2044, 1996.

[131] G. E. Yakubov, B. Loppinet, H. Zhang, J. Rühe, R. Sigel, and G. Fytas. Collective dynamics of an end-grafted polymer brush in solvents of varying quality. *Phys. Rev. Lett.*, 92:115501, 2004.

[132] J. Abbou, A. Agnés, and C. Demaille. Accessing the dynamics of end-grafted flexible polymer chains by atomic force-electrochemical microscopy. Theoretical modeling of the approach curves by the elastic bounded diffusion model and Monte Carlo simulations. Evidence for compression-induced lateral chain escape. *J. Phys. Chem. B*, 110:22664–22675, 2006.